약학박사학위논문

Factors Affecting Pharmacokinetics of Edaravone after Oral Administration: Solubilization and Efflux Transport

렛드에서 에다라본의 경구 흡수를 결정짓는 주요 요소들에 대한 연구

2019년 2월

서울대학교 대학원

약학과 약제과학 전공

형 성 우

ABSTRACT

Factors Affecting Pharmacokinetics of Edaravone after Oral Administration: Solubilization and Efflux Transport

Sungwoo Hyung

Department of Pharmaceutical Science

College of Pharmacy

The Graduate School

Seoul National Univesity

This study was performed to determine the primary factor(s) governing the oral absorption of edaravone, a novel anti-oxidant for the treatment of amyotrophic lateral sclerosis, in rats. While the aqueous solubility of edaravone widely varied depending on the vehicle used, the oral bioavailability of the drug was not low when it was adequately solubilized, as evidenced by the fact that the oral exposure was high (in terms of the absolute bioavailability of 50 - 90%) at all dose ranges (i.e., 0.5 - 27 mg/kg) under solubilized conditions in rats. The sum of the in vitro clearance values for

edaravone, 12.7 mL/(min×kg), obtained from metabolic stability studies with tissue-homogenates from the rat liver, kidney, intestine, and with the rat plasma, was found to be virtually identical to the systemic clearance of the drug in rats. It was noted that the liver represented over 83.9% of the total elimination with a hepatic extraction ratio of approximately 0.137, indicative of the minor role of hepatic first pass metabolism in the systemic absorption of edaravone after its oral administration. In studies with Ussing chamber with rat intestinal segments and Madin-Darby canine kidney (MDCKII) cells, edaravone was found to be highly permeable (i.e., P_{app} over 10 x 10^{-6} cm/sec),and appeared to be a substrate for rat P-glycoprotein (P-gp; estimated K_m of 421 μM). Incontrast, however, the drug did not appear to be a substrate for human P-gp in transport studies with MDCKII-hMDR1 cells. When incorporating the kinetic parameters for the *in vitro* studies like as metabolism, permeability, and P-gp efflux into physiologically based pharmacokinetics models, the characteristics of edaravone plasma profiles were consistent with the findings of the *in vivo* study. Collectively, these observations suggest that the primary determining factor for the intestinal absorption of edaravone is its solubilization in vehicle/intestinal fluids, rather than permeability, pre-systemic first-pass metabolism, or efflux transport. Considering the fact that the newly approved indication of the drug would require prolonged administration, probably via oral administration, the findings reported herein provide relevant information regarding its use. Additionally, when this study is considered together with the study of the species-difference in OCT2 stimulation (Appendix), both studies suggest that

the species-difference in drug transporter can be meaningful to understand the pharmacokinetics of the drugs.

Keywords : Edaravone, Pharmacokinetics, Oral absorption, Bioavailability, P-glycoprotein, Species-difference, In vitro – In vivo extrapolation

Student Number : 2014-30566

Contents

List of Figures

List of Tables

1. Introduction

Edaravone (3-methyl-1-phenyl-2-pyrazolin-5-one, Radicava/Radicut®), a free radical scavenger, was originally developed for the treatment of acute strokes (Kikuchi et al., 2013; Lapchak, 2010; Watanabe et al., 2008; Yoshida et al., 2006). Since the treatment of a brain infarction would necessitate an acute exposure of the drug, the only reasonable route of the administration would be intravenous (iv) administration via infusion at a dose of 30 mg twice a day for 14 days (i.e., approximately 1 mg/kg/day for humans) (Lapchak, 2010; Sinha et al., 2009). The intravenous infusion of edaravone was also recently approved for the treatment of amyotrophic lateral sclerosis (i.e., Lou Gehrig's disease), a chronic and neurodegenerative disease, by the United States Food and Drug Administration (FDA) (Abe et al., 2017; Hardiman and van den Berg, 2017; Yoshino and Kimura, 2006). For the case of this new application, however, an oral administration, rather than parenteral administration, would be preferable, since amyotrophic lateral sclerosis is a chronic disease. Unfortunately, however, an oral formulation of edaravone was not commercially available currently, although such a form of edaravone (TW001) is currently under development/study in the form of a phase 1 clinical study (Mohamed et al., 2017). The pharmacokinetic characteristics for the experimental formulation have not yet been published in the literature. Pre-formulation / formulation studies, however, have been carried out for edaravone (Parikh et al., 2016, 2017; Rong et al., 2014), including the

determination of its oral bioavailability in rats: It was found that the oral bioavailability of edaravone was reported to be quite low (i.e., 5.23%) in rats (Rong et al., 2014), suggesting that this pharmacokinetic insufficiency could be a major limiting factor for the development of an oral formulation for this drug. However, Rong et al. (2014) reported on the bioavailability by comparing the systemic exposure in rats that were receiving markedly different dosage levels via different administration routes (i.e., an oral dose at 27 mg/kg vs an iv dose at 9 mg/kg). Furthermore, the dosage used in the study was quite high in comparison to the recommended clinical dosage: As a reference, the approved dose for human use in clinical practice would be close to 1 mg/kg (60 mg per day), and, even if the pharmacokinetic data based on a rat brain ischemia model were compared to humans (Doi et al., 2004; SHIBATA et al., 1998; Takamatsu et al., 1997), the dosage would not exceed 3 mg/kg. Considering the fact that the underlying mechanism by which edaravone is absorbed across the intestine is not fully understood, the difference in the dosage between the two administration routes may have affected the estimation of the oral bioavailability of the drug. In addition, the results of single-pass intestinal perfusion studies with rats indicate that the permeability of edaravone is enhanced by a co-treatment with verapamil, a standard inhibitor of the P-glycoprotein (P-gp), suggesting P-gp mediated efflux is involved in the transport of edaravone across the rat intestine (Rong et al., 2014): Obviously, the involvement of P-gp mediated efflux in this process would be expected to limit the bioavailability of the drug and would have an effect on its estimation. In addition to the potential involvement of an

efflux process, the limited dissolution of the drug in the dosing solution and/or the intestinal fluid may also contribute to the low oral bioavailability in rats, since the drug has limited solubility in aqueous media [1.85 mg/mL, (Parikh et al., 2017)]. Based on the above findings, it is clear that the determining factor(s) that govern the low oral bioavailability of edaravone are not completely understood.

The results of routine pharmacokinetics studies suggest that the oral bioavailability of edaravone vastly exceeds the estimates reported in the literature (i.e., approximately 5%; Rong et al., 2014) in rats receiving a clinical dosage of the drug in the range of 0.5 - 5 mg/kg. Considering the differences in the experimental designs, the kinetic discrepancies may be manifested by multiple factors. The objective of the study, therefore, was to identify the primary factor(s) that govern the oral bioavailability of this antioxidant in the rats regarding four major aspects of oral absorption, i.e., solubility, metabolism, permeability, and P-gp mediated efflux.

2. Materials and Methods

2.1. Chemicals and Reagents

Verapamil, metoprolol, and digoxin were purchased from Sigma-Aldrich (St Louis, USA). Edaravone (3-methyl-1-phenyl-5-pyrazolone) was obtained from Tokyo Chemical Industry Co., Ltd. (Tokyo, Japan). Radiolabeled [3H]-digoxin (specific activity: 29.8 Ci/mmol; PerkinElmer Life or Analytical Sciences (MA,USA) was also used in this study. All other chemicals were of the highest grade available and were used without further purification.

2.2. Animal

Male Sprague-Dawley (SD) rats [7–8 weeks old: Orient Bio Inc. (Gyeonggi-do, Korea)] were housed under a 12 h light/dark cycle for equilibration, and fasted overnight before the animal experiments (i.e., all in vivo studies and the collection of blood / tissue samples). The protocols for all animal studies were reviewed and approved by the Institutional Animal Care and Use Committees of Seoul National University, Seoul, Republic of Korea, according to the guidance (Number 85-23), Principles of Laboratory Animal Care (revised in 1985), from the National Institutes of Health Publication.

2.3. Dose-ranging Study

Dose dependent pharmacokinetic studies were performed according to previously described methods (Jeong et al., 2017; Lee et al., 2015a; Ryu et al., 2017). Briefly, male SD rats, weighing 235–250 g, were anesthetized by an intramuscular administration of 40 mg/kg tiletamine-HCl/zolazepam-HCl (Zoletil 50) and 10 mg/kg xylazine-HCl (Rompun). After confirming the induction of anesthesia, the femoral artery (for collecting blood samples) and vein (for administering and supplementing body fluids) were catheterized with polyethylene tubing (PE 50; Clay Adams, Parsippany, NJ) filled with heparinized saline (20 U/mL; for arterial cannulae) and normal saline (for venous cannulae), respectively. Edaravone was dissolved in saline containing 2% DMSO and the solution administered via intravenous / oral routes at doses of 0.5, 1, 2, and 5 mg/kg (the volume of the dosing solution was fixed at 2 mL/kg for both routes). Blood samples (150 μL) were collected in heparinized tubes via the right femoral artery at 2, 5, 15, 30, 60, 90, 120, 180, and 240 min after being administered to rats. Immediately after blood collection, a volume of saline identical to the volume of the blood sample was administered to the animal to compensate for the fluid loss. Plasma samples, obtained by the centrifugation of blood samples at 16,100 g for 5 min at 4˚C, were collected and the concentration of the drug in the plasma was determined using an LC-MS/MS assay for edaravone (see 2.10).

2.4. High-dose *In vivo* Study

To determine whether the bioavailability of edaravone at higher dose could

be enhanced by the improved solubilization of edaravone, in vivo pharmacokinetic study was carried out with saline containing 2% DMSO as the vehicle in rats (see 2.3). In this supplementary study, the dose of edaravone was set at 9 mg/kg for intravenous bolus, and 27 mg/kg for oral administrations, as used in the literature (Rong et al., 2014). In addition, the volume of dosing solution was 2 mL/kg for IV, and 6 mL/kg for po administration.

2.5. Solubility Study

In this study, the solubility of edaravone in various aqueous vehicles was determined using a previously described method (Parikh et al., 2016; Yin et al., 2009b). In this study, the test vehicles included double distilled water, 0.5% sodium carboxymethyl cellulose (CMC-Na) [for an in vivo study in the literature (Parikh et al., 2016; Rong et al., 2014)], 2% DMSO in saline (the primary vehicle used in this study), simulated gastric fluid, and simulated intestinal fluid. For solubility measurements, an excess amount of edaravone was added into 1 mL of test vehicle, followed by mixing in a shaking incubator at 25˚C for 24 h. The solution was then centrifuged at 16,100 g for 5 min at room temperature: The supernatant was filtered to remove excess edaravone, and the concentration of the drug in the filtrate was determined by an LC-MS/MS assay (see 2.10).

2.6. Stability of Edaravone in Tissue Homogenates and

Plasma of the Rat

In this study, the metabolic stability of edaravone was determined in homogenates of the liver, kidney, and intestine from the rats using procedures described in the literature (Ao et al., 2015; Lee et al., 2016). Tissue-homogenate was selected as proper metabolic assay system for edaravone because the main metabolites of the drug are its sulfate and glucuronide form (SHIBATA et al., 1998), so it is essential to evaluate phase 2 metabolism. Also, it was reported that the kidney may contribute the metabolism of edaravone (Ma et al., 2012), this tissue was included in experimental design with the liver and intestine which are related with first-pass metabolism. Briefly, after recovering from the anesthesia, the rats were immediately sacrificed by cervical dislocation for the collection of the liver, kidney, and intestine. The wet weight of tissue was determined, and the tissue sample was then homogenized in a 2-fold volume of Dulbecco's phosphate-buffered saline using a homogenizer (Ultra Turrax model, T25, IKA Works, Inc, Cincinnati, OH). An aliquot (499 μL) of pre-warmed (37˚C) tissue homogenate was mixed with 1 μL of a solution containing 5 mM edaravone for the initiation of the metabolic reaction: The mixture was incubated at 37˚C and aliquots (50 μL) of the homogenate were collected at various times (i.e., at 0, 5, 10, 15, and 20 min). The concentration of the drug in the sample was immediately determined using an LC-MS/MS assay (see 2.10) and the percent of edaravone remaining in the incubation determined.

When it was necessary to assess the stability of edaravone in the plasma, a

blood sample was collected from the rat and the plasma was prepared as described above. An aliquot (499 μL) of pre-warmed (37˚C) plasma was then mixed with 1 μL of a solution containing the drug (final concentration of edaravone to be 10 μM) for the initiation of the reaction. The mixture was incubated at 37˚C, and aliquots (50 μL) of the incubate was sampled at various times (i.e., at 0, 5, 10, 15, and 20 min). The concentration of the drug in the sample was immediately determined using an LC-MS/MS assay (see 2.10) and the percent of edaravone remaining in the incubation determined.

The unbound fraction of edaravone in the rat plasma ($f_{u,p}$) or in tissue homogenate ($f_{u,tissue}$) was also determined in this study by an ultrafiltration technique, essentially as described in the literature (Berry et al., 2009). Because it was aimed to evaluate the unbound fraction of the drug in potential metabolic tissues, rapid equilibrium dialysis (RED) method was not recommended.

When necessary, intrinsic clearance ($CL_{intrinsic}$, mL/min) was estimated using data obtained from metabolic stability studies using the following equation (1).

$$CL_{int} = \frac{\mathrm{k}}{D} \times tissue\ weight \cdots\cdots\cdots equation\ (1)$$

where k represents the rate constant for the metabolic elimination of the drug [i.e., obtained from the half-life ($t_{1/2}$) of the percent remaining vs. the time curve using the relationship $k = 0.693/t_{1/2}$] and D is the fold dilution estimated

from the tissue weight contained in the incubation and anatomical tissue weight. In addition, 'tissue weight' indicated in the equation represents the anatomical tissue weight for the liver, kidney, intestine, and plasma for a 250 g rat. For the case of plasma, 'tissue weight' represents the product of the anatomical volume of blood of a 250 g rat and 1-hematocrit (i.e., the hematocrit was assumed to be 0.45 in this study).

When it was necessary to convert CL_{int} to extraction ratio (ER), the following equation was used.

$$\mathrm{ER} = \frac{\frac{CL_{int}}{f_{u,tissue}} \times f_{u,p}}{(Q_T \times R + \frac{CL_{int}}{f_{u,tissue}} \times f_{u,p})} \cdots\cdots\cdots equation\ (2)$$

where $f_{u,p}$ is the unbound fraction of edaravone in the rat plasma, $f_{u,tissue}$ is the unbound fraction of the drug in the tissue homogenate, Q_T is the blood flow to the tissue, and R is the blood to plasma concentration ratio. In this study, R was assumed to be unity. Tissue clearance of edaravone (CL_{tissue}) was calculated by using equation (3).

$$CL_{tissue} = Q_T \times R \times ER \cdots\cdots\cdots equation\ (3)$$

2.7. Ussing chamber study

To determine if a carrier-mediated process is involved in the transport of

edaravone across the rat intestine, Ussing chamber study was carried out according to a procedure described in the literature (Lee et al., 2005; Stephens et al., 2001; Yin et al., 2009a) with minor modifications. Briefly, a segment of the ileum was carefully dissected from an anesthetized rat and the excised tissue was immediately added to freshly prepared transport medium with O_2/CO_2 (95:5) bubbling. The isolated segment was cut along the mesenteric borderline to expose the luminal side and the serous membrane isolated. The membrane was then mounted on a diffusion chamber. After assembling the chamber, the mounted membrane was pre-incubated with pre-warmed (37˚C) transport media for 20 min. The medium was then replaced by 37˚C pre-warmed media without (i.e., receiver side), or with edaravone (10, 50, 100, 500, and 1000 μM for donor side). If necessary, verapamil (500 μM, final concentration) was also added at the donor side to determine if a P-gp mediated process is involved in the transport of edaravone across the rat intestine. In our preliminary study, we found that the presence of 500 μM verapamil was sufficient to inhibit digoxin transport to an extent similar to that reported in the literature (Stephens et al., 2001) in our Ussing chamber studies. The tissue was further incubated at 37˚C with constant O2/CO2 (95:5) bubbling: Samples from the receiver (0.1 mL per sample) were collected for 30, 60, 90, and 120 min after the initiation of the transport reaction with the replenishment of the medium. The apparent permeability of edaravone for the rat ileum was determined using the following equation.

$$P_{app} = \frac{dQ}{dt} \times \frac{1}{A} \times \frac{1}{C_0} \ldots\ldots\ldots equation\ (4)$$

where dQ/dt is the rate of transport, A is the surface area of the membrane, and C_0 is the initial concentration of edaravone in the donor side.

When it was necessary to analyze the kinetics of the concentration-dependent transport of edaravone in Ussing chamber studies, the following equation (Nerurkar et al., 1997) was used. In this kinetic analysis, the parallel first-order kinetics for the absorptive direction and saturable process in the secretory direction (i.e., efflux), as described by simple Michaelis-Menten kinetics, were assumed to be involved in the overall permeability (P_{app}) of edaravone:

$$P_{app} = P_{passive} - P_{saturable} \ldots\ldots\ldots equation\ (5)$$

$$P_{saturable} = \frac{J_{max}}{(K_m + [S])} \ldots\ldots\ldots equation\ (6)$$

where $P_{passive}$ represents the passive permeability of edaravone, $P_{saturable}$ is the saturable efflux of edaravone, J_{max} is the maximal flux of edaravone across the rat intestine, K_m is the Michaelis-Menten constant, and [S] is the concentration of the drug in the donor side. In this study, metoprolol, a highly permeable marker (FDA, 2015) [i.e., the estimated permeability of 6 - 20 x 10^{-6} cm/sec, (Patel et al., 2006; Roos et al., 2017)], was used as a positive control for the transport study in the Ussing chamber studies.

2.8. MDCKII-hMDR1 Permeability and Transport Assay

In this study, MDCKII cells expressing the human P-gp (human multidrug resistance protein 1, MDCKII-hMDR1 cells), a gift from the Netherlands Cancer Institute (Amsterdam, the Netherlands), was used. Cell culture conditions and the conditions for the transport study for edaravone were virtually identical to those described previously with slight modifications (Hyung et al., 2017; Lee et al., 2015b; Yim et al., 2017). Briefly, MDCKII-hMDR1 cells were grown in Dulbecco's modified Eagle's medium with 10% (v/v) fetal bovine serum, a 1% (v/v) non-essential amino acid solution, 100 units/mL penicillin/streptomycin, and 10 mM HEPES. All cells were kept at 37˚C with 5% CO_2 and 95% relative humidity. Cells were seeded at a density of 2 × 105 cells/well on collagen-coated 12 mm Transwell® plates (Costar, Corning, New York), and the medium replaced at 2-day intervals. A bi-directional transport study was then carried out on the 6th day after seeding. The confluence of the cell monolayer and the integrity of the tight junction were confirmed by microscopic observations and measurement of transepithelial electrical resistance (TEER; 154-183 Ω) (Irvine et al., 1999). The cells were washed twice and pre-incubated with transport medium (9.7 g/L Hanks' balanced salts, 2.38 g/L HEPES, and 0.35 g/L sodium bicarbonate, pH adjusted to 7.4) for 30 min at 37°C. For the inhibition study, the basolateral to apical and the apical to basolateral transport of edaravone were measured in the presence and the absence of verapamil 500 μM (i.e., a P-gp inhibitor).

The transport buffer containing only edaravone (i.e., 1, 10, and 100 μM) or edaravone with the inhibitor was added to the donor chamber (0.5 mL for the apical chamber or 1.5 mL for the basolateral chamber). Pre-warmed (at 37˚C), drug-free transport buffer was added to the receiver chamber and the cells were incubated at 37°C. In this study, the final concentration of the organic solvent (e.g., DMSO) in the transport buffer was fixed at 0.1% in all experiments. In our previous study, it was found that concentrations of DMSO of up to 2% in the transport medium had no appreciable effect on the function of the MDCKII cells expressing drug transporter (Yim et al., 2017), consistent with other literature findings (Da Violante et al., 2002; Taub et al., 2002). An aliquot (300 μL for apical chamber or 500 μL for basolateral chamber) of the media was collected from the receiver chamber at 120 min. The concentration of the drug in the sample was determined using an LC-MS/MS assay (see 2.10). To determine the functionality of P-gp in the cells, the transport of digoxin, a known P-gp substrate, was studied in parallel: [^{3}H]-Digoxin, along with unlabeled digoxin (to minimize non-specific binding; the total final concentration of digoxin to be 1 μM), was added to the donor chamber and a transport study carried out similar to that described above. In both transport studies, an aliquot (300 μL for the apical chamber or 500 μL for the basolateral chamber) of media was collected from the receiver chamber at 120 min after the start of the incubation and transferred to a fresh scintillation vial. An aliquot (1 mL) of scintillation fluid [Ultima Gold (Perkin-Elmer Life Science)] was added to the vial, and the amount of edaravone was determined by liquid scintillation counting (Tri-Carb 3110 TR, Perkin-Elmer Life

Science). In transport studies, the apparent permeability coefficient (P_{app}, in 10^{-6} cm/sec) was calculated using equation (4).

When necessary, the efflux ratio was also determined by the following equation, using the apparent permeability from the basolateral to the apical direction ($P_{app,\ B\ to\ A}$) and the apparent permeability from the apical to basolateral direction ($P_{app,\ A\ to\ B}$):

$$\text{Efflux ratio} = \frac{P_{app,B\ to\ A}}{P_{app,A\ to\ B}} \ldots\ldots\ldots equation\ (7)$$

2.9. ATPase assay

To study whether the transport of edaravone was mediated by human and/or rat P-gp, an ATPase assay, as indirect evidence of the P-gp mediated transport, was carried out by Corning® Gentest™ ATPase Assay Kit (Corning), according to the instructions from the manufacturer (Drueckes et al., 1995; Sarkadi et al., 1992). Briefly, insect cell (BTI-TN5B1-4) membranes containing hMDR1 or rMDR1a (Corning) were plated at 96-well microplate. In this study, the membrane was treated with edaravone (i.e., 1 or 100 μM), with the MgATP solution as the source of ATP for 30 min. The liberation of inorganic phosphate, the by-product of ATPase activity, was measured by UV spectrophotometry at 800 nm. In this supplementary study, verapamil, a known substrate of P-gp, was used as a standard substrate for the efflux transporter (i.e., positive control), and sodium orthovanadate was used as a

reference inhibitor of ATPase (Ambudkar et al., 1992; Kimura et al., 2007).

2.10. Determination of Edaravone Concentration by LC-MS/MS Assay

The concentrations of edaravone in various samples were determined by an LC-MS/MS method. An aliquot (50 μL) of a sample was added to 200 μL of a mixed solvent [i.e., methanol (MeOH) and 0.1% (v/v) formic acid] containing glipizide (100 ng/mL, internal standard), and the mixture vortexed for 5 min. The mixture was then centrifuged (16,100g for 5 min at 4˚C) and an aliquot (5 μL) of the supernatant was then directly injected onto the LC-MS/MS system (Applied Biosystems 3200 Qtrap MS/MS system with Alliance Waters e2695 LC system): The mobile phase, consisting of 0.1% formic acid in acetonitrile (mobile phase A) and 0.1% formic acid in purified water (mobile phase B), was delivered at a flow rate of 0.5 mL/min using a gradient elution involving 30% of A (0 minutes), from 30% to 95% of A (0 - 0.1 minutes), 95% of A (0.1 - 0.6 minutes), from 95% to 30% of A (0.6 - 0.7 minutes), and 30% of A (0.7 - 5 minutes). Chromatographic separation was carried out on an HPLC column [SynergiTM Polar-RP 80 Å, 4 μM, 2 × 150 mm, Phenomenex, Torrance, CA)] at 25°C while the temperature in the autosampler was maintained at 4°C during the analysis. Samples were ionized using a turbo ion spray interface in the positive ionization mode and monitored at the following MRM conditions at m/z 175.1 -> 65.1 for

edaravone, and 445.8 -> 320.9 for glipizide. The pressure of the curtain gas, ion spray voltage, source temperature, ion source gas 1, and ion source gas 2 were 30 psi, 5500 V, 450°C, 40 psi, and 30 psi, respectively. The declustering potential, entrance potential, collision energy and collision cell exit potential were 41.0 V, 11.5 V, 41.0 V, and 4.0 V, respectively. In this study, the precision and accuracy were found to be within the acceptance criteria in the guidelines of assay validation (FDA, 2013).

2.11. Statistical Analysis

To compare the means between treatments, the two-tailed unpaired Student's t test or one-way ANOVA was used. When necessary, nonlinear regression and moment analyses were carried out using the Winnonlin® Professional 5.0.1 software (Pharsight Corporation, Mountain View, CA) and GraphPad Prism version 5.01 (GraphPad Software Inc., San Diego, CA). In this study, data are expressed as the mean ± S.D. and a $p<0.05$ was accepted as denoting statistical significance.

2.12. Physiologically Based Pharmacokinetic Modeling of Edaravone

In this study, 3 anatomical tissues (viz, liver, kidney, and intestine) and 1 theoretical tissue (carcass) for rats were included in the PBPK calculations.

Input parameters are listed in Table 4 and were used in the calculation of the plasma concentration-time relationship. In this study, the pharmacokinetic model of edaravone was assume to follow perfusion-limited model because its passive permeability was evaluated as high in Ussing chamber study and MDCKII permeability assay. Also, intestinal lumen comparment was included for oral administration group with P-gp efflux interactions on the drug's absorption. A simulation was carried out with Berkeley Madonna software (version 8.3.18; University of California, Berkeley, CA). In this study, the fourth order of the Runge-Kutta method was used for the numerical integration.

For the case of the liver;

$$V_L \frac{dC_L}{dt} = (Q_L - Q_I) \cdot R \cdot C_{art} + Q_I \cdot \frac{C_I}{K_{p,I}} - Q_L \cdot \frac{C_L}{K_{p,L}} - CL_{int,L} \times C_L \dots\dots\dots equation\ (8)$$

where V_L is the volume of liver tissue; C_L, C_I, and C_{art} are the drug concentration in the liver, intestine, and arterial blood; Q_L, Q_I are the blood flow to the liver and intestine; $K_{p,L}$ and $K_{p,I}$ are the tissue-to-plasma concentration ratio for the liver and intestine; $CL_{int,L}$ is the intrinsic clearance in liver tissue.

For the case of the kidney;

$$V_K \frac{dC_K}{dt} = Q_K \cdot R \cdot C_{art} - Q_K \cdot R \cdot \frac{C_K}{K_{p,K}} - CL_{int,K} \cdot C_K \ldots\ldots\ldots equation\ (9)$$

where V_K is the volume of kidney tissue; C_K is the drug concentration in the kidney; Q_K is the blood flow to the kidney; $K_{p,K}$ is the tissue-to-plasma concentration ratio for the kidney; and $CL_{int,k}$ is the intrinsic clearance in kidney tissue.

For the case of the intestine at the iv administration group;

$$V_I \frac{dC_I}{dt} = Q_I \cdot R \cdot C_{art} - Q_I \cdot R \cdot \frac{C_I}{K_{p,I}} - CL_{int,I} \cdot C_I \ldots\ldots\ldots equation\ (10)$$

where V_I is the volume of intestine tissue; $CL_{int,I}$ is the intrinsic clearance in intestine tissue.

For the case of the intestine at the oral administration group;

$$V_I \frac{dC_I}{dt} = Q_I \cdot R \cdot C_{art} - Q_I \cdot R \cdot \frac{C_I}{K_{p,I}} - CL_{int,I} \cdot C_I + PS_{uptake} \cdot C_{lumen}$$

$$\ldots\ldots\ldots equation\ (11)$$

where C_{lumen} is the drug concentration in intestinal fluid; PS_{uptake} is the intestinal absorption clearance of the drug.

For the case of the intestinal lumen at the oral administration group;

$$V_{lumen}\frac{dC_{lumen}}{dt} = Dose - PS_{uptake} \cdot C_{lumen} \ldots\ldots\ldots equation\ (12)$$

where V_{lumen} is the volume of intestinal fluid;

For the case of the carcass;

$$V_C\frac{dC_C}{dt} = Q_C \cdot R \cdot C_{art} - Q_C \cdot R \cdot \frac{C_C}{K_{p,C}} \ldots\ldots\ldots equation\ (13)$$

where V_C is the volume of carcass compartment; C_C is the drug concentration in the carcass; Q_C is the blood flow to the carcass; $K_{p,C}$ is the tissue-to-plasma concentration ratio for the carcass;

For the case of the arterial blood;

$$V_{art}\frac{dC_{art}}{dt} = Q_{CO} \cdot R \cdot C_{ve} - Q_{CO} \cdot R \cdot C_{art} - CL_{int,p} \cdot C_{art} \ldots\ldots\ldots equation\ (14)$$

where V_{art} is the volume of arterial blood; C_{ve} is the venous plasma concentration of drug; Q_{CO} is the cardiac output; $CL_{int,p}$ is the intrinsic clearance in plasma;

For the case of the venous blood at the iv administration group;

$$V_{ve}\frac{dC_{ve}}{dt} = Q_K \cdot R \cdot \frac{C_K}{K_{p,K}} + Q_L \cdot \frac{C_L}{K_{p,L}} + Q_C \cdot R \cdot \frac{C_C}{K_{p,C}} - Q_{CO} \cdot R \cdot C_{ve} + Dose\ rate \ldots\ldots\ldots equation\ (15)$$

For the case of the venous blood at the oral administration group;

$$V_{ve}\frac{dC_{ve}}{dt} = Q_K \cdot R \cdot \frac{C_K}{K_{p,K}} + Q_L \cdot \frac{C_L}{K_{p,L}} + Q_C \cdot R \cdot \frac{C_C}{K_{p,C}} - Q_{CO} \cdot R \cdot C_{ve}$$

$$\ldots\ldots\ldots equation\ (16)$$

where V_{ve} is the volume of venous blood;

K_{pC} value was calculated from this equation

$$V_{ss} = V_p + \sum_{i=1}^{i=n} V_{tissue,i} \cdot K_{p,ss,i} \ldots\ldots\ldots equation\ (17)$$

$$K_{pC} = \frac{(V_{ss}\text{-}V_p - V_L \cdot K_{pL,ss} - V_K \cdot K_{pK,ss} - V_I \cdot K_{pI,ss})}{V_c} \ldots\ldots\ldots equation\ (18)$$

where $K_{pL,ss}$, $K_{pK,ss}$, and $K_{pI,ss}$ is the tissue-to-plasma concentration ratio at steady state for liver, kidney, and intestine. These values were calculated from this equation;

$$K_{p,ss} = K_p \cdot (1 - ER)$$

$$= \frac{f_{u,p}}{f_{u,t}} \cdot \frac{Q_T \times R}{(Q_T \times R + \frac{CL_{int}}{f_{u,tissue}} \times f_{u,p})} \ldots\ldots\ldots equation\ (19)$$

PS_{uptake} was derived from this equation;

$$PS_{uptake} = P_{app} \cdot SA \ldots\ldots\ldots equation\ (20)$$

where P_{app} is the apparent permeability of edaravone via intestinal absorption, and SA is the intestinal lumen surface area. These parameters were derived from this equations;

$$P_{app} = P_{passive} - \frac{J_{max}}{K_m + C_{lumen}} \ldots\ldots\ldots equation\ (21)$$

$$fragment_{surface\ area} = \pi \cdot fragment_{length} \cdot fragment_{diameter}$$

$$\ldots\ldots\ldots equation\ (22)$$

$$SA = Duo_{surface\ area} + Jeju_{surface\ area} + Ile_{surface\ area}$$

$$\ldots\ldots\ldots equation\ (23)$$

3. Results

3.1. Dose-dependency of Edaravone Pharmacokinetics in Rats

Temporal profiles for the concentration of edaravone in the plasma after its administration via an iv bolus or the oral route at doses of 0.5, 1, 2, and 5 mg/kg to rats are shown in Fig. 1. In general, the profiles decreased in a multi-exponential fashion: Pharmacokinetic parameters, estimated from non-compartmental analysis, are summarized in Table 1. For the case of the iv administration study, the CLtotal for edaravone was not significantly different with the edaravone dose, suggesting that the elimination of the antioxidant is mediated by linear kinetics. The V_{ss} of edaravone did not vary in the dosage range of 0.5 - 2 mg/kg, although the parameter was slightly elevated at 5 mg/kg ($p<0.05$, one-way ANOVA, followed by Tukey's post hoc test).

For the case of the oral administration study, the dose normalized AUCpo values from 0.5 and 1 mg/kg dose appeared to be quite different from those at doses of 2 and 5 mg/kg, although a statistical difference was not detected for the kinetic parameter amongst the dosage levels, probably because of the large variability associated. Interestingly, we noted that the extent of absorption was not low (over 50%) in the dose levels studied (i.e., from 0.5 - 5 mg/kg), which is in direct contradiction to existing literature reports (i.e., approximately 5.23%, Rong et al., 2014). To determine whether the intestinal absorption is a function of the dosing vehicle, a high dose study was carried

out using a vehicle that adequately solubilized the antioxidant (Fig. 6). When the absolute bioavailability was calculated using 9 mg/kg for the iv and 27 mg/kg for the oral routes [i.e., the dosage identical to that used in the reference (Rong et al., 2014)], the value was estimated to be 82.0% (Table 3) which was much higher than the reported value of 5.23% (Rong et al., 2014). The marked difference in bioavailability appeared to be related to the difference in the vehicle used [i.e., low bioavailability when using a 0.5% sodium carboxymethyl cellulose (CMC-Na) suspension (Rong et al., 2014)] where the drug may not have been completely soluble (see 3.2 and 4).

3.2. Solubility Study

Since the solubility of edaravone may be a factor in its intestinal absorption, the solubility of the drug was screened in various vehicles (Fig. 2). The intrinsic aqueous solubility of edaravone was 1.17 ± 0.359 mg/mL: A value that was not significantly different from the solubility of the drug in 0.5% CMC-Na (1.52 ± 0.473 mg/mL). Edaravone [pKa of 7.0, (Watanabe et al., 2008)], was more soluble in the acidic simulated gastric fluid (SGF, pH 1.2; 3.02 ± 0.36 mg/mL) than in the simulated intestinal fluid (SIF, pH 6.8; 2.24 ± 0.15 mg/mL) solution. The solubility of edaravone was significantly enhanced in saline containing 2% DMSO (7.78 ± 0.361 mg/mL), compared to its intrinsic aqueous solubility. In this study, saline containing 2% DMSO was used as the primary dosing vehicle unless otherwise noted.

3.3. Metabolic Stability in Tissue Homogenates and the Plasma of the Rat

In this study, metabolic stability of edaravone was determined in homogenates derived from three different tissues (i.e., the intestine, kidney, and liver) and in the plasma of the rat (Fig. 3). The apparent tissue clearance (CLtissue) of edaravone, estimated from equation (3), the unbound fraction (Table 2), and the intrinsic clearance (CL_{int}) [i.e., see equation (1)], was determined to be 0.277 ± 0.0650, 0.182 ± 0.0239, and 2.65 ± 0.204 mL/min in the rat intestine, kidney, and liver, respectively. In addition, the clearance of the drug from plasma was estimated to be 0.0481 ± 0.0114 mL/min. If we assume that the drug is eliminated exclusively via metabolism [i.e., the renal elimination of edaravone would be below 2% in rats, (KOMATSU et al., 1996)] and the three organs / the plasma are the primary metabolizing sites for edaravone, the theoretical total clearance (i.e., $CL_{total,\ theoretical}$) can be estimated from the summation of CL_{tissue} and CL_{plasma}. Accordingly, the CL_{total}, theoretical was 3.17 mL/min for a 250 g rat [or 12.7 mL/min/kg], a value that was quite comparable to that found in in vivo (i.e., $CL_{total,\ in\ vivo}$ to be from 11.2 to 13.8 mL/min/kg, Table 1). The physiological/biopharmaceutical parameters used in the equations are listed in Table 2.

3.4. Transport Studies and Permeability Measurements for

Edaravone

Ussing chamber studies were carried out with the rat ileum to estimate the permeability of edaravone across the rat intestine. The apparent permeability of metoprolol (i.e., a highly permeable marker) at a concentration of 30 μM in the donor compartment was estimated to be $10.9 \pm 1.56 \times 10^{-6}$ cm/sec. This value was essentially identical to that reported in other studies (Patel et al., 2006; Roos et al., 2017), suggesting that our experimental system is adequate for measuring the apparent permeability across the rat intestine. For the case of 10 μM edaravone, the absorptive permeability in the rat ileum was found to be $7.12 \pm 2.18 \times 10^{-6}$ cm/sec and this value was significantly enhanced to $15.6 \pm 4.84 \times 10^{-6}$ cm/sec ($p<0.05$) when a co-treatment with 500 μM verapamil was used, suggesting that the efflux pathway for edaravone is blocked by verapamil (viz, a P-gp inhibitor). Consistent with this finding, the concentration dependency for absorptive permeability (Fig. 4) indicates the involvement of saturable efflux with linear influx, as expressed in equations (5 and 6). A nonlinear regression analysis of the data with the kinetic model indicated that K_m, J_{max}, and $P_{passive}$ values of 421 μM, 2.17 ng/(sec x cm^2), and 32.2×10^{-6} cm/sec, respectively, best described our results. Taken together, these observations suggest that the anti-oxidant may interact with the rat P-gp, as has been suggested in previous studies (Rong et al., 2014).

In this study, the permeability of edaravone was also determined in MDCKII cells expressing hMDR1 (Fig. 5). When digoxin, a known P-gp substrate, was used as a positive control, its apparent permeability was found to be 0.966 ±

0.0292×10^{-6} cm/sec for $P_{app, A\ to\ B}$, and $12.7 \pm 2.15 \times 10^{-6}$ cm/sec for $P_{app, B\ to\ A}$, respectively. In the presence of the co-treatment with verapamil, a known P-gp inhibitor, the permeability values were altered to $3.54 \pm 0.260 \times 10^{-6}$ cm/sec for Papp, A to B and $3.88 \pm 0.175 \times 10^{-6}$ cm/sec for Papp, B to A, respectively. As a result, the efflux ratio of digoxin was reduced from 13.2 to 1.10 in the case of a co-treatment with verapamil, indicating that the P-gp functions adequately in MDCKII cells expressing hMDR1. When the $P_{app, A\ to\ B}$ and $P_{app\ B\ to\ A}$ values were determined at three different concentrations of edaravone, the efflux ratios of edaravone were found to be 0.838, 0.909, and 0.852 for 1, 10, and 100 μM of the drug (Fig. 5), respectively. Considering the fact that the threshold for the involvement of efflux transport is generally considered to be an efflux ratio value greater than 2 (Zhang et al., 2008), it would appear that edaravone is unlikely to be a substrate for human P-gp. Furthermore, the P_{app} values of edaravone was not affected by the presence of verapamil (Fig. 5): The efflux ratios of edaravone were 0.592, 0.790, and 0.731 in the presence of verapamil, respectively. Taken together, the apparent permeability and efflux ratio of edaravone were relatively unaltered by the co-treatment of verapamil in MDCKII-hMDR1 cells, thus suggesting that edaravone is not a substrate for human P-gp. The P_{app} values were declined at low edaravone concentration (1 μM) by poor recovery. It was observed that the recovery drops to 70% within only 30 sec after treating the drug as same way. This observation suggests that nonspecific binding induced poor recovery at the low concentration group.

Different experimental system was used to evaluate human P-gp (MDCKII)

and rat P-gp (Ussing chamber). To exclude the possibility that the species-difference in P-gp efflux was induced by using different systems, the ATPase activity for human P-gp or rat P-gp in the presence and the absence of edaravone were also determined (Fig. 7). NaOV-sensitive ATPase activity was significantly enhanced by verapamil, a known P-gp substrate, indicating that the two membrane systems function adequately. However, the addition of edaravone (i.e., 1 and 100 μM, final concentration) failed to enhance ATPase activity in the membrane containing hMDR1, whereas 100 μM edaravone significantly enhanced NaOV-sensitive ATPase activity in an rMDR1a membrane, compared to the control group [in nmole/(mg protein x min), 4.81 ± 1.47 without edaravone and 56.2 ± 14.6 with 100 μM edaravone] (Fig. 7). Therefore, our observations regarding ATPase activity assay are consistent with the hypothesis that edaravone is a substrate for rat P-gp, but not for human P-gp.

3.5. Simulation of Edaravone Pharmacokinetics after a Intravenous or Oral Administration in Rats Using a PBPK model

In this study, we attempted to use a PBPK model to predict the plasma concentration of edaravone at the dose of 1 mg/kg and 5 mg/kg for iv and po administration groups using primarily *in vitro* experimental results (Fig. 8). Our calculations indicate that the profiles for the plasma concentration of the

drug could be reasonably predicted when the drug was given to rats by iv or po routes (Fig. 9). Sensitivity analysis was done to evaluate the significant changes of the profiles by the change of each factors (Fig. 10).

4. Discussion

The objective of the current study was to identify the major factor(s) governing the intestinal absorption of edaravone. Considering the fact that the therapeutic application of the drug is now being extended to amyotrophic lateral sclerosis (Hardiman and van den Berg, 2017), a chronic disease, the development of an adequate oral formulation may be important for its pharmacotherapeutic use. Indeed, a number of formulation studies for edaravone have been recently reported (Parikh et al., 2016, 2017; Rong et al., 2014). However, the primary biopharmaceutical mechanism(s) limiting the intestinal absorption of the antioxidant were not completely delineated.

In a recent study, the oral bioavailability of edaravone was reported to be low (i.e., approximately 5%) in rats (Rong et al., 2014): In the study reported by Rong et al. (2014), the drug was apparently given to rats in the form of a suspension dispersed in 0.5% CMC-Na. The findings reported herein indicate that the solubility of edaravone in 0.5% CMC-Na is 1.52 mg/mL [Fig. 2; as a reference, the literature value of 1.89 mg/mL (Parikh et al., 2017)]. Therefore, the vehicle would not be able to sufficiently solubilize the drug to produce a formulation adequate for oral administration to rats. In this study, we were able to solubilize the drug up to an edaravone concentration of 7.78 mg/mL in 2% DMSO in saline (i.e., the primary vehicle used in this study, Fig. 2). Using the dosage reported by Rong et al. (2014) as the reference (i.e., an iv dosage at 9 mg/kg and an oral dosage at 27 mg/kg), the bioavailability with the solubilized edaravone was now estimated to be approximately 82.0%

(Table 3). Considering the fact that a high oral bioavailability was consistently found for the drug in the oral dosage range of 0.5 - 27 mg/kg (Table 1, Table 3), an adequate solubilization of edaravone is likely to be one of the determining factors for its intestinal absorption.

In this study, we found the elimination of edaravone is largely mediated by linear pharmacokinetics. It should be noted, however, that the tissue distribution of the drug may deviate somewhat from linear kinetics at a higher dose since the steady state volume of distribution was slightly elevated in the case of an iv dose of 5 mg/kg (i.e., the highest dose): We found that this potential nonlinear pharmacokinetics was observed only when the blood concentration exceeded 9300 ng/mL. As a comparison, the maximal blood concentration obtained with the oral administration in this study was much lower (6800 ng/mL), suggesting that the tissue distribution of edaravone can be described by linear kinetics in the range of concentration achieved by oral administration with the studied dosage levels examined here. Under these kinetic conditions, we noted that the oral bioavailability appeared to be considerably elevated at higher dosages (Table 1), suggesting that nonlinear absorption is potentially involved in the intestinal absorption of the drug. Since it was previously reported that edaravone served as a substrate of rat P-gp (Rong et al., 2014), it appeared reasonable to hypothesize that the elevated bioavailability at the higher dosages is related to the action of the efflux transporter in rats. Consistent with this statement, our Ussing chamber study with rat intestinal tissues showed that the serosal to luminal efflux was saturable at a K_m of 421 μM (Fig. 4). Assuming the total intestinal fluid

volume in rats to be approximately 3.2 mL (McConnell et al., 2008), the estimated concentration of edaravone in the intestine would be at least 700 μM with a dose of 2 mg/kg (i.e., the lowest dosage showing elevated bioavailability), suggesting that efflux transport may be partially saturated in the case of the oral administration of edaravone at the dosage higher than 2 mg/kg. This assumption can be supported by sensitivity analysis in PBPK calculation that variation in parameters related to efflux transport induced significant profile changes at 1 mg/kg PO group, however, not at 5 mg/kg PO group where the transporter-mediated efflux was already saturated (Fig. 9). As a corollary proof, we found that the addition of edaravone enhanced the utilization of ATP in rMDR1a-expressing membranes (Fig. 7). Therefore, these observations suggest that efflux transporters in the rat intestine, such as P-gp, participate in the intestinal absorption of edaravone.

It was previously reported that edaravone was primarily metabolized to its sulfate and glucuronide metabolites (KOMATSU et al., 1996), indicating that uridine 5'-diphospho-glucuronosyltransferase and sulfotransferases are involved in the elimination process (Ma et al., 2012; Mizuno et al., 2007b; YOKOTA et al., 1997). These metabolizing enzymes are reported to be present in the liver, kidney, and intestine in rats (Krishna and Klotz, 1994). To determine the kinetics of the phase II metabolisms in those organs, the metabolic stability in tissue-homogenates was measured for the organs for the elimination of edaravone in rats. We were particularly interested in the stability of the drug in the homogenates of the liver and intestine (for the estimation of pre-systemic/systemic elimination), and the kidney (for the

partial estimation of systemic elimination) (Ma et al., 2012). In addition, the metabolic stability of the drug was measured in the rat plasma (Fig. 3). The summation of CL_{liver}, CL_{kidney}, $CL_{intestine}$, and CL_{plasma} resulted in 3.17 mL/min for a 250 g rat [i.e., 12.7 mL/(min×kg)]: This value was virtually identical to the in vivo systemic clearance of the drug in the dose range of 0.5 - 5 mg/kg (Table 1), suggesting that these organs (i.e., the liver, kidney, intestine, and plasma) largely account for the elimination of edaravone in rats. In addition, amongst these organs, the value for CLtissue was the highest for the liver, indicating that the liver represents the primary organ for eliminating edaravone in rats and that the extent of contribution is minimal for the other tissues (Table 2). Nonetheless, the extraction ratio (ER) value calculated from the liver was low (i.e., 0.137 ± 0.0105, Table 2), indicating that hepatic first-pass metabolism is not high nor is it the major factor in the oral absorption of edaravone.

Since edaravone is a known substrate for rat P-gp (Rong et al., 2014), this transporter may act as an important barrier for the intestinal absorption of the drug. Interestingly, we found that the apparent permeability of edaravone was high in MDCKII cells expressing hMDR1 (i.e., $P_{app, A\ to\ B}$ and $P_{app, B\ to\ A}$ values exceeding 10×10^{-6} cm/sec, at all test concentrations, Fig. 5), suggesting that edaravone is highly permeable (Irvine et al., 1999; Varma et al., 2005), even in cells expressing hMDR1. As a result, the efflux ratio of edaravone was less than 1 at all concentrations in MDCKII cells expressing hMDR1. Furthermore, the efflux ratio was not affected by a co-treatment with verapamil, a known P-gp inhibitor, suggesting that, although edaravone is

subjected to efflux transport by rat P-gp, the drug is not transported by human P-gp. It should also be noted that the addition of edaravone did not enhance the utilization of ATP in hMDR1-expressing membrane (Fig. 7). Species-differences in transport processes for drug transporters (Chu et al., 2013), including P-gp (Syvanen et al., 2009), are well documented. For example, we recently reported that species-differences in the stimulation of organic cation transporter 2 exist between human and rats in in vitro cell models (Hyung et al., 2017). Since edaravone and its metabolites are reported to interact with various drug transporters (Mizuno et al., 2007a; Mizuno et al., 2007b), further studies regarding the possibility of species-difference(s) in other transporter(s) with edaravone are warranted.

5. Conclusion

In conclusion, the oral bioavailability of edaravone was found to be not low (i.e., over 50%) in rats in the dose range from 0.5 to 27 mg/kg, if the drug is adequately solubilized. Secondary to aqueous solubility, edaravone was subjected to be transported by an efflux transporter in the rat intestinal membrane, most likely via rat P-gp. However, the drug did not appear to interact with human P-gp, suggesting that P-gp mediated efflux is not the major determining factor in the development of oral formulations of edaravone for use in humans. In addition, the passive permeability was found to be high while intestinal/hepatic first-pass metabolism appeared to be low in the intestinal absorption of edaravone in rats. Considering the fact that the newly approved indication of the drug would require chronic administration, most likely orally, the current study may be pharmaceutically relevant.

6. References

Abe, K., et al., 2017. Safety and efficacy of edaravone in well defined patients with amyotrophic lateral sclerosis: a randomised, double-blind, placebo-controlled trial. The Lancet Neurology 16, 505-512.

Ambudkar, S.V., et al., 1992. Partial purification and reconstitution of the human multidrug-resistance pump: characterization of the drug-stimulatable atp hydrolysis. Proceedings of the National Academy of Sciences 89, 8472-8476.

Ao, L., et al., 2015. Polymer micelle formulations of proteasome inhibitor carfilzomib for improved metabolic stability and anticancer efficacy in human multiple myeloma and lung cancer cell lines. Journal of Pharmacology and Experimental Therapeutics 355, 168-173.

Berry, L.M., et al., 2009. Prediction of Vss from in vitro tissue binding studies. Drug Metabolism and Disposition, dmd. 109.029629.

Chu, X., et al., 2013. Species differences in drug transporters and implications for translating preclinical findings to humans. Expert Opinion on Drug Metabolism and Toxicology 9, 237-252.

Da Violante, G., et al., 2002. Evaluation of the cytotoxicity effect of dimethyl sulfoxide (DMSO) on Caco2/TC7 colon tumor cell cultures. Biological & Pharmaceutical Bulletin 25, 1600-1603.

Doi, K., et al., 2004. Radical scavenger edaravone developed for clinical use ameliorates ischemia/reperfusion injury in rat kidney. Kidney International 65, 1714-1723.

Drueckes, P., et al., 1995. Photometric microtiter assay of inorganic phosphate in the presence of acid-labile organic phosphates. Analytical Biochemistry 230, 173-177.

FDA, 2013. FDA guidance for industry: bioanalytical method validation. US Department of Health and Human Services, Food and Drug Administration, Center for Drug Evaluation and Research (CDER).

FDA, 2015. Draft guidance for industry. Waiver of in vivo bioavailability and bioequivalence studies for immediate-release solid oral dosage forms based on a biopharmaceutics classification system. Available at:)(Accessed May 18, 2015) http://www. fda. gov/downloads/Drugs/Guidances/ucm070246. pdf Date.

Hardiman, O., van den Berg, L.H., 2017. Edaravone: a new treatment for ALS on the horizon? Lancet Neurology 16, 490-491.

Hyung, S., et al., 2017. The conditional stimulation of rat organic cation transporter 2, but not its human ortholog, by mesoridazine: the possibility of the involvement of the high-affinity binding site of the transporter in the stimulation. Journal of Pharmacy and Pharmacology 69, 1513-1523.

Irvine, J.D., et al., 1999. MDCK (Madin-Darby Canine Kidney) cells: a tool for membrane permeability screening. Journal of Pharmaceutical Sciences 88, 28-33.

Jeong, Y.S., et al., 2017. Estimation of the minimum permeability coefficient in rats for perfusion-limited tissue distribution in whole-body physiologically-based pharmacokinetics. European Journal of Pharmaceutics and Biopharmaceutics 115, 1-17.

Kikuchi, K., et al., 2013. Edaravone (radicut), a free radical scavenger, is a potentially useful addition to thrombolytic therapy in patients with acute ischemic stroke (review). Biomedical reports 1, 7-12.

Kimura, Y., et al., 2007. Modulation of drug-stimulated ATPase activity of human MDR1/p-glycoprotein by cholesterol. Biochemical Journal 401, 597-605.

KOMATSU, T., et al., 1996. Pharmacokinetic studies of 3-methyl-1-phenyl-2-pyrazolin-5-one-(MCI-186): metabolism in rats, dogs and human. Drug Metabolism and Pharmacokinetics 11, 451-462.

Krishna, D.R., Klotz, U., 1994. Extrahepatic metabolism of drugs in humans. Clinical Pharmacokinetics 26, 144-160.

Lapchak, P.A., 2010. A critical assessment of edaravone acute ischemic stroke efficacy trials: is edaravone an effective neuroprotective therapy? Expert Opinion on Pharmacotherapy 11, 1753-1763.

Lee, H.T., et al., 2005. Prokinetic activity of an aqueous extract from dried immature fruit of Poncirus trifoliata (L.) Raf. Journal of Ethnopharmacology 102, 131-136.

Lee, J.H., et al., 2015a. The identification of lobeglitazone metabolites in rat liver microsomes and the kinetics of the in vivo formation of the major metabolite M1 in rats. Journal of Pharmaceutical and Biomedical Analysis 115, 375-382.

Lee, J.H., et al., 2015b. Kinetics of the absorption, distribution, metabolism, and excretion of lobeglitazone, a novel activator of peroxisome proliferator-activated receptor gamma in rats. Journal of Pharmaceutical Sciences 104,

3049-3059.

Lee, J.Y., et al., 2016. High body clearance and low oral bioavailability of alantolactone, isolated from Inula helenium, in rats: extensive hepatic metabolism and low stability in gastrointestinal fluids. Biopharmaceutics & Drug Disposition 37, 156-167.

Ma, L., et al., 2012. Glucuronidation of edaravone by human liver and kidney microsomes: biphasic kinetics and identification of UGT1A9 as the major UDP-glucuronosyltransferase isoform. Drug Metabolism and Disposition 40, 734-741.

McConnell, E.L., et al., 2008. Measurements of rat and mouse gastrointestinal pH, fluid and lymphoid tissue, and implications for in-vivo experiments. Journal of Pharmacy and Pharmacology 60, 63-70.

Mizuno, N., et al., 2007a. Human organic anion transporters 1 (hOAT1/SLC22A6) and 3 (hOAT3/SLC22A8) transport edaravone (MCI-186; 3-methyl-1-phenyl-2-pyrazolin-5-one) and its sulfate conjugate. Drug Metabolism and Disposition 35, 1429-1434.

Mizuno, N., et al., 2007b. Evaluation of the role of breast cancer resistance protein (BCRP/ABCG2) and multidrug resistance-associated protein 4 (MRP4/ABCC4) in the urinary excretion of sulfate and glucuronide metabolites of edaravone (MCI-186; 3-methyl-1-phenyl-2-pyrazolin-5-one). Drug Metabolism and Disposition 35, 2045-2052.

Mohamed, L.A., et al., 2017. Blood-brain barrier driven pharmacoresistance in amyotrophic lateral sclerosis and challenges for effective drug therapies. AAPS Journal 19, 1600-1614.

Nerurkar, M.M., et al., 1997. Mechanistic roles of neutral surfactants on concurrent polarized and passive membrane transport of a model peptide in Caco-2 cells. Journal of Pharmaceutical Sciences 86, 813-821.

Parikh, A., et al., 2016. Development of a novel oral delivery system of edaravone for enhancing bioavailability. International Journal of Pharmaceutics 515, 490-500.

Parikh, A., et al., 2017. Lipid-based nanosystem of edaravone: development, optimization, characterization and in vitro/in vivo evaluation. Drug Deliv 24, 962-978.

Patel, N., et al., 2006. Use of simulated intestinal fluids with Caco-2 cells and rat ileum. Drug Development and Industrial Pharmacy 32, 151-161.

Rong, W.T., et al., 2014. Hydroxypropyl-sulfobutyl-β-cyclodextrin improves the oral bioavailability of edaravone by modulating drug efflux pump of enterocytes. Journal of Pharmaceutical Sciences 103, 730-742.

Roos, C., et al., 2017. Regional intestinal permeability in rats: a comparison of methods. Molecular Pharmaceutics 14, 4252-4261.

Ryu, H.M., et al., 2017. Quantification of EC-18, a synthetic monoacetyldiglyceride (1-palmitoyl-2-linoleoyl-3-acetyl-rac-glycerol), in rat and mouse plasma by liquid-chromatography/tandem mass spectrometry. Journal of Pharmaceutical and Biomedical Analysis 137, 155-162.

Sarkadi, B., et al., 1992. Expression of the human multidrug resistance cDNA in insect cells generates a high activity drug-stimulated membrane ATPase. Journal of Biological Chemistry 267, 4854-4858.

SHIBATA, H., et al., 1998. Phase I clinical study of MCI-186 (edaravone, 3-methyl-1-phenyl-2-pyrazolin-5-one) in healthy volunteers. Rinsho yakuri/Japanese Journal of Clinical Pharmacology and Therapeutics 29, 863-876.

Sinha, M.K., et al., 2009. Edaravone in acute ischemic stroke, an indian experience. Neurology Asia 14, 7-10.

Stephens, R.H., et al., 2001. Kinetic profiling of P-glycoprotein-mediated drug efflux in rat and human intestinal epithelia. Journal of Pharmacology and Experimental Therapeutics 296, 584-591.

Syvanen, S., et al., 2009. Species differences in blood-brain barrier transport of three positron emission tomography radioligands with emphasis on P-glycoprotein transport. Drug Metabolism and Disposition 37, 635-643.

Takamatsu, Y., et al., 1997. Studies on the concentrations of 3-methyl-1-phenyl-2-pyrazolin-5-one (MCI-186) in MCA occlusion and reperfusion model of rats. Japanese Pharmacology and Therapeutics 25, 275-282.

Taub, M.E., et al., 2002. Optimized conditions for MDCK permeability and turbidimetric solubility studies using compounds representative of BCS classes I–IV. European Journal of Pharmaceutical Sciences 15, 331-340.

Toutain, P.-L., BOUSQUET-MÉLOU, A., 2004a. Plasma terminal half-life. Journal of Veterinary Pharmacology and Therapeutics 27, 427-439.

Toutain, P.-L., BOUSQUET-MÉLOU, A., 2004b. Volumes of distribution. Journal of Veterinary Pharmacology and Therapeutics 27, 441-453.

Varma, M.V., et al., 2005. Functional role of P-glycoprotein in limiting

intestinal absorption of drugs: contribution of passive permeability to P-glycoprotein mediated efflux transport. Molecular Pharmaceutics 2, 12-21.

Watanabe, T., et al., 2008. The novel antioxidant edaravone: from bench to bedside. Cardiovasc Ther 26, 101-114.

Yim, C.S., et al., 2017. Specific inhibition of the distribution of lobeglitazone to the liver by atorvastatin in rats: evidence for a rat organic anion transporting polypeptide 1b2-mediated interaction in hepatic transport. Drug Metabolism and Disposition 45, 246-259.

Yin, Y.M., et al., 2009a. Preparation, characterization and in vitro intestinal absorption of a dry emulsion formulation containing atorvastatin calcium. Drug Deliv 16, 30-36.

Yin, Y.M., et al., 2009b. Docetaxel microemulsion for enhanced oral bioavailability: preparation and in vitro and in vivo evaluation. Journal of Controlled Release 140, 86-94.

YOKOTA, S., et al., 1997. A pharmacokinetic study of MCI-186, a novel drug for cerebrovascular disease in elderly and young healthy subjects. Rinsho yakuri/Japanese Journal of Clinical Pharmacology and Therapeutics 28, 693-702.

Yoshida, H., et al., 2006. Neuroprotective effects of edaravone: a novel free radical scavenger in cerebrovascular injury. CNS Drug Reviews 12, 9-20.

Yoshino, H., Kimura, A., 2006. Investigation of the therapeutic effects of edaravone, a free radical scavenger, on amyotrophic lateral sclerosis (phase II study). Amyotrophic Lateral Sclerosis 7, 241-245.

Zhang, L., et al., 2008. A regulatory viewpoint on transporter-based drug

interactions. Xenobiotica 38, 709-724.

국문초록

본 연구의 목적은, 근위축성 측삭 경화증 (루게릭병)의 치료에 사용되는 중요 항산화제인 에다라본의 경구 흡수에 중요하게 작용하는 요인이 무엇인지를 렛드에서 알아보는 것이다. 우선 에다라본의 용해도는 용매에 따라 크게 달라지는 것을 확인하였다. 이 중 적절한 용매를 이용하여 에다라본을 완전히 용해시킨 경우, 이 약물의 생체이용률은 결코 낮지 않다는 것을 관찰하였다. 이것은 0.5 – 27 mg/kg 용량 범위에서 절대 생체이용률이 50 – 90%에 달하는 것으로부터 확인할 수 있었다. *In vitro* 클리어런스 값을 렛드의 간, 신장, 소장, 혈장으로부터 구한 합이 12.7 mL/(min×kg)였고 이 값은 *in vivo* 렛드 실험에서 구한 총 클리어런스 값과 거의 같았다는 점에서, 해당 실험계가 *in vivo* 상황을 잘 반영함을 알 수 있었다. 또한 간에서의 클리어런스가 이 약물의 총 클리어런스의 83.9%에 해당하는 것에서 간이 주된 대사 장기임을 알 수 있었다. 하지만 간에서의 extraction ratio가 0.137에 불과하단 점에서, 경구 투여시 초회 통과 대사의 영향은 크지 않다는 것을 알 수 있었다. 렛드의 소장을 이용한 Ussing chamber study와 MDCKII 세포주를 이용한 투과도 실험에서, 에다라본은 투과도가 높은 약물이며 (P_{app} 값이 10 x 10^{-6} cm/sec 이상), 렛드의 P–

glycoprotein의 기질성을 보임을 알 수 있었다 (K_m 값, 421 μM). 하지만 MDCKII-hMDR1 세포주를 이용한 실험에서 에다라본은 인간의 P-glycoprotein의 기질은 아닌 것을 알 수 있었다. 대사, 투과도, P-gp efflux와 같은 *in vitro* 실험에서 얻은 결과값을 PBPK modeling에 도입하였을 때, 예측된 에다라본의 혈중 농도 곡선은 *in vivo*에서 구한 결과에 부합하였다.

위 결과들을 종합하면 에다라본의 경구 흡수에는 투과도, 초회 통과 대사, efflux transporter의 영향은 크지 않았으며, 약물을 적절한 용매에 용해시키는 것이 가장 중요하게 작용한다는 것을 알 수 있었다. 이 약물의 새로운 적응증인 근위축성 측삭 경화증에는 경구 제제를 이용한 장기 복용이 효과적일 것이기에, 이 연구는 이와 관련하여 중요한 역할을 할 것으로 보인다. 추가적으로, 이 연구 결과를 OCT2 stimulation의 종간 차이에 대한 연구와 종합했을 때 (Appendix), 약물 수송체의 종간 차이가 약물의 동태학적 연구에 있어 중요하게 작용할 수 있음을 알 수 있었다.

주요어 : 에다라본, 약물동태, 경구 흡수, 생체이용률, P-glycoprotein, 종차, in vitro - in vivo 연관성

Table 1. Pharmacokinetics parameters of edaravone in the dose ranging study in rats.

Route	**iv**				**po**			
Dose (mg/kg)	**0.5**	**1**	**2**	**5**	**0.5**	**1**	**2**	**5**
T_{max} (min)	-	-	-	-	3.00 ± 1.73	5.00 ± 0.00	5.00 ± 0.00	8.33 ± 5.77
$t_{1/2}$ (min)	15.7 ± 2.20	17.4 ± 5.53	19.7 ± 2.96	35.0 ± 7.96	-	-	-	-
C_{max} (ng/mL)	-	-	-	-	938 ± 478	1330 ± 304	5710 ± 6280	6810 ± 3340
AUC_{inf} (μg×min/mL)	38.6 ± 1.87	83.7 ± 2.39	192 ± 6.58	391 ± 128	21.7 ± 7.73	46.6 ± 15.8	180 ± 104	353 ± 68.9
AUC_{inf}/dose (10^{-4}×kg×min/mL)	772 ± 37.0	837 ± 23.9	958 ± 32.9	783 ± 25.6	435 ± 15.5	466 ± 158	900 ± 518	706 ± 138
CL_{total} [mL/(min×kg)]	13.0 ± 0.610	12.6 ± 3.47	11.2 ± 3.20	13.8 ± 4.90	-	-	-	-
V_{ss} (mL/kg)	250 ± 29.2	242 ± 29.0	261 ± 55.1	405 ± 71.9	-	-	-	-
BA (%)	-	-	-	-	56.3	55.6	93.9	90.1

The iv/po AUC data for the matching dose were used for the calculation of BA for the dose level. Data are expressed as the mean ± S.D. from triplicate runs.

Table 2. Summary of pharmacokinetic and physiological parameters for a tissue-homogenate metabolic study.

	Liver	Kidney	Intestine	Plasma	Reference
k (min^{-1})	0.124 ± 0.0112	0.0720 ± 0.00958	0.0563 ± 0.0137	0.00571 ± 0.00135	
Tissue weight (g)	8.57	2.19	6.19	8.43	(Jeong et al., 2017)
$CL_{int,invitro}$ (mL/min)	3.19 ± 0.288	0.473 ± 0.0629	1.05 ± 0.254	-	
$f_{u,tissue}$,$f_{u,p}$	0.173	0.425	0.606	0.167	
Extraction ratio	0.137 ± 0.0105	0.0157 ± 0.00206	0.0343 ± 0.00804	-	
Q_T (mL/min)	19.4	11.6	8.08	-	(Jeong et al., 2017)
CL_{tissue} (mL/min)	2.65 ± 0.204	0.182 ± 0.0239	0.277 ± 0.0650	0.0481 ± 0.0114	

Data are expressed as the mean ± S.D. from quadruplicate runs.

Table 3. The pharmacokinetic parameters of edaravone at higher doses

Route	**iv**	**po**
Dose (mg/kg)	9	27
T_{max} (min)	-	6.33 ± 7.51
$t_{1/2}$ (min)	45.6 ± 10.6	-
C_{max} (ng/mL)	-	31700 ± 31600
AUC_{inf} (min×μg/mL)	477 ± 49.5	1170 ± 951
CL_{total} [mL/(min×kg)]	18.6 ± 1.86	-
V_{ss} (mL/kg)	630 ± 99.1	-
BA (%)	-	82.0

Table 4. Summary of kinetic parameters for edaravone used in PBPK calculation.

Parameter	Values	Systems	References
$f_{u,p}$	0.167	Ultrafiltration	Determined
$f_{u,L}$	0.173	Ultrafiltration	Determined
$f_{u,K}$	0.425	Ultrafiltration	Determined
$f_{u,I}$	0.606	Ultrafiltration	Determined
R	1	-	-
Q_L (mL/min)	19.4	-	SimCYP
Q_K (mL/min)	11.6	-	SimCYP
Q_I (mL/min)	8.08	-	SimCYP
Q_{CO} (mL/min)	80	-	SimCYP
k_{liver} (1/min)	0.124	Tissue-homogenate	Determined
k_{kidney} (1/min)	0.072	Tissue-homogenate	Determined
$k_{intestine}$ (1/min)	0.0563	Tissue-homogenate	Determined
k_{plasma} (1/min)	0.00571	Tissue-homogenate	Determined
J_{max} (ng/[sec×cm^2])	2.17	Ussing chamber	Determined
K_m (μM)	421	Ussing chamber	Determined
$P_{passive}$ (cm/sec)	32.2×10^{-6}	Ussing chamber	Determined
Molecular weight	174.2	-	Pubchem
Duo_{length} (cm)	7	-	SimCYP
$Duo_{diameter}$ (cm)	0.275	-	SimCYP
$Jeju_{length}$ (cm)	90	-	SimCYP
$Jeju_{diameter}$ (cm)	0.4	-	SimCYP
Ile_{length} (cm)	20	-	SimCYP
$Ile_{diameter}$ (cm)	0.4	-	SimCYP

V_{lumen} (mL)	3.2	-	McConnell et al.,(2008)
V_L (mL)	8.57	-	SimCYP
V_K (mL)	2.19	-	SimCYP
V_I (mL)	6.19	-	SimCYP
V_{ve} (mL)	15.32×2/3	-	SimCYP
V_{art} (mL)	15.32×1/3	-	SimCYP
V_{ss} (mL/kg) at 1 mg/kg	242	*in vivo*	Determined
V_{ss} (mL/kg) at 5 mg/kg	405	*in vivo*	Determined

Table 5. Comparison of pharmacokinetic parameter from observed and simulated plasma concentration-time profiles of edaravone.

Route	IV					
Dose	1 mg/kg			5 mg/kg		
	Observed	Simulated	Ratio (fold)	Observed	Simulated	Ratio (fold)
AUC_{last} (μg×min/mL)	76.8	75.4	0.98	383	400	1.04
AUC_{inf} (μg×min/mL)	83.7	79.6	0.95	391	400	1.02
V_{ss} (mL/kg)	242	215	0.89	405	435	1.07
Route	PO					
Dose	1 mg/kg			5 mg/kg		
	Observed	Simulated	Ratio (fold)	Observed	Simulated	Ratio (fold)
AUC_{last} (μg×min/mL)	41.3	56.1	1.36	335	330	0.99
AUC_{inf} (μg×min/mL)	46.6	63.8	1.37	353	332	0.94
Cmax (ng/mL)	1330	1080	0.81	6810	5109	0.75

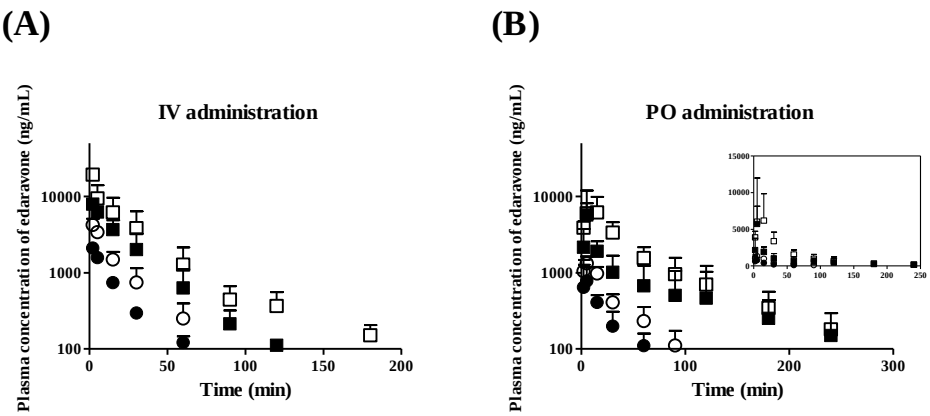

Figure 1. Temporal profiles for the plasma concentration of edaravone after intravenous bolus or oral administrations.

The doses of edaravone were 0.5 (●), 1 (○), 2 (■), and 5 (□) mg/kg for iv (A) or po (B) administration routes. Plasma samples were collected at 2, 5, 15, 30, 60, 90, 120, 180, and 240 min. Data points represent the mean ± S.D. from triplicate runs.

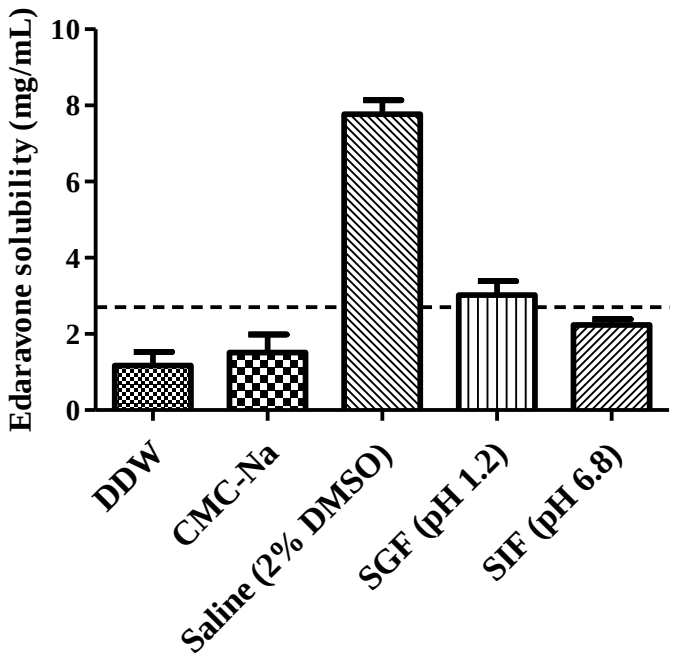

Figure 2. Solubility of edaravone in various aqueous vehicles.

A dotted line represents the expected concentration of edaravone in 0.5% CMC-Na at an edaravone dose of 27 mg/kg, assuming the maximum recommended volume (10 mL/kg) of dosing solution (McConnell et al., 2008) is applied. Bars represent the mean ± S.D. from quadruplicate runs.

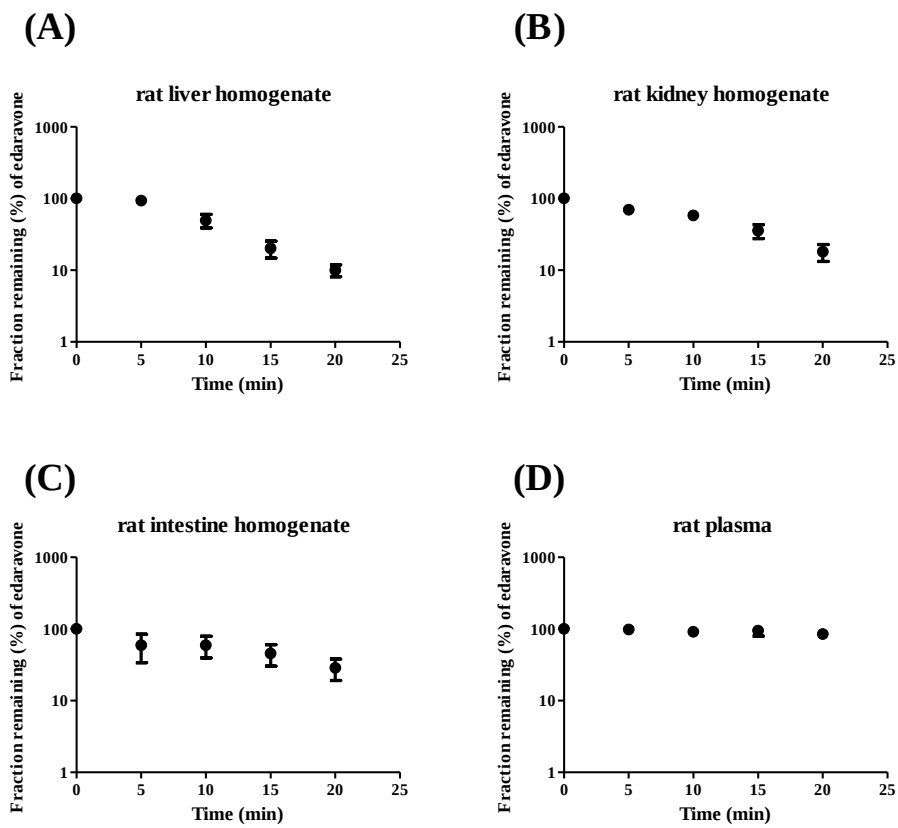

Figure 3. Metabolic stability of edaravone in rat tissue homogenates. Temporal profiles of edaravone remaining in homogenates of the rat liver (A), kidney (B), intestine (C), and in the rat plasma (D). Rat tissue homogenates and plasma were incubated with 10 μM edaravone up to 20 min at 37˚C. Data points represent the mean ± S.D. from quadruplicate runs.

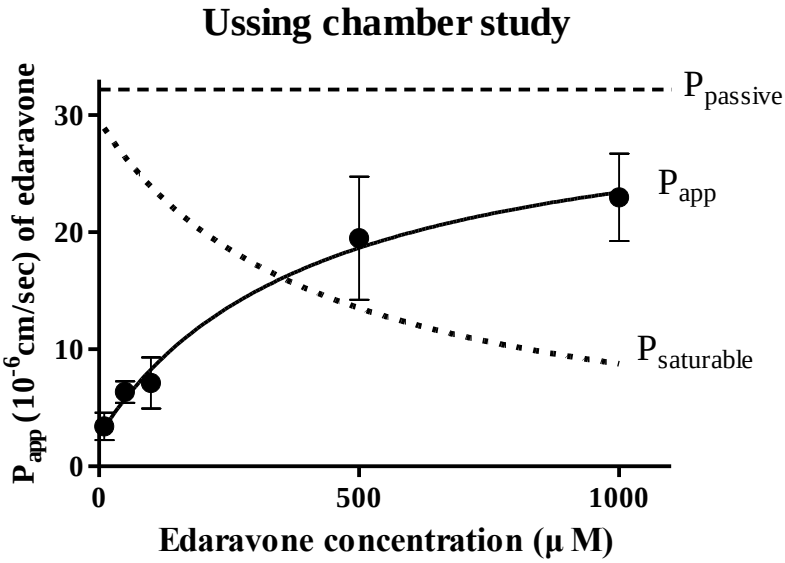

Figure 4. Concentration-dependent permeability profile of edaravone in Ussing chamber study with the rat ileum fragment.

Apparent permeability of edaravone was determined at 37˚C for 120 min at various concentrations (10, 50, 100, 500, and 1000 μM). The solid line was generated from the nonlinear regression analysis of the permeability data with equations (5 and 6, see section 2.6). The dotted lines represent the portion of the permeability for the passive influx and of the saturable efflux of edaravone, calculated from the nonlinear regression analysis. Data points represent the mean ± S.D. from quadruplicate runs.

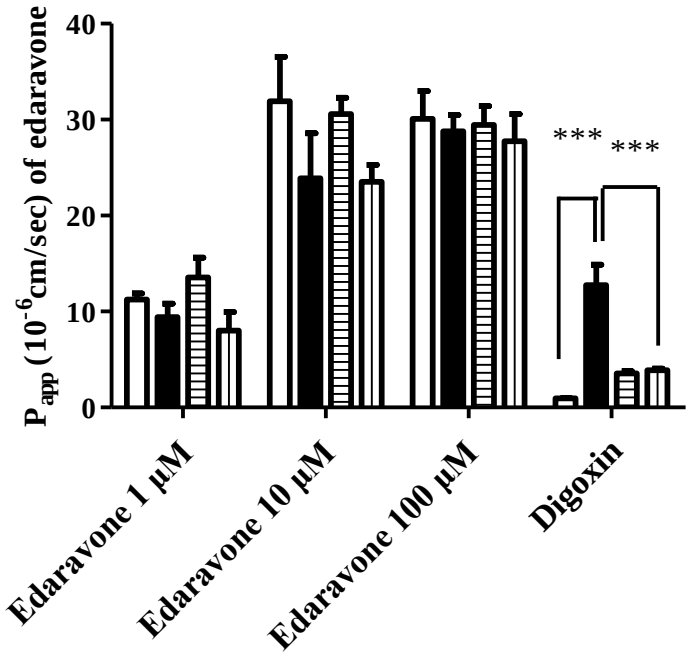

Figure 5. The apparent permeability of edaravone in MDCK-hMDR1 cells. The rate of transport of 1, 10, and 100 μM edaravone (i.e., apical to basolateral or basolateral to apical) was determined in MDCK-hMDR1 cells with (i.e., horizontally striped bars for $P_{app, A\ to\ B}$ and vertically striped bars for $P_{app, B\ to\ A}$) or without (i.e., blank bars for $P_{app, A\ to\ B}$ and filled bars for $Pa_{pp, B\ to\ A}$) 500 μM verapamil. In this study, the results from 1 μM digoxin transport are also presented as a positive control. Bars represent the mean ± S.D. from triplicate runs. Key: ***, $p<0.001$ by one-way ANOVA, followed by Tukey's post hoc test.

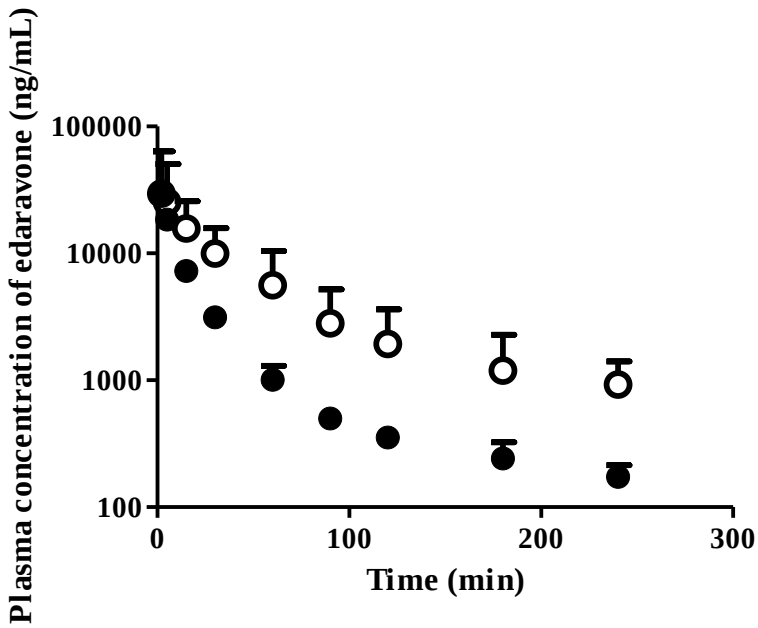

Figure 6. Profiles for the plasma concentration of edaravone after an intravenous bolus or oral administration.

The doses of edaravone was 9 mg/kg for intravenous bolus (●), and 27 mg/kg for oral administration (○). The plasma samples were collected at 2, 5, 15, 30, 60, 90, 120, 180, and 240 min. Data points represent the mean ± S.D. from triplicate runs.

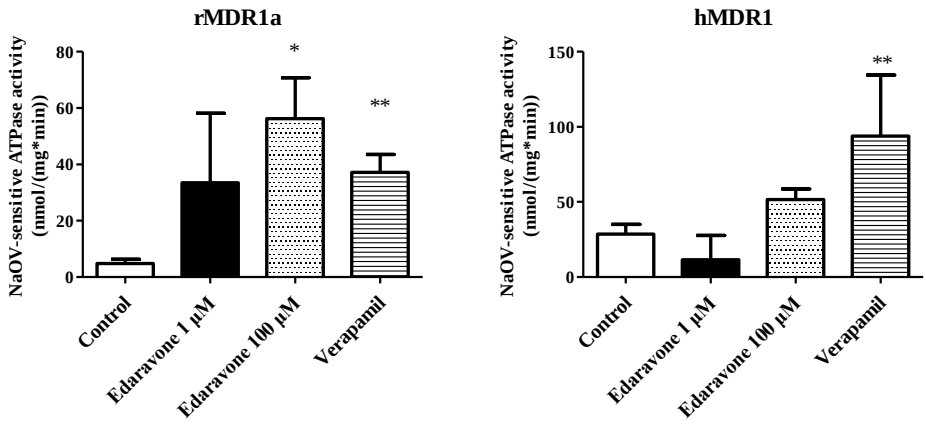

Figure 7. ATPase activity in insect cell membranes containing hMDR1 and rMDR1a in the presence and the absence of edaravone.

NaOV-sensitive ATPase activities were determined when the membrane was treated with edaravone [i.e., 1 (i.e., filled bar) or 100 μM (i.e., dotted bar)]. Blank bar represents a negative control, and verapamil (i.e., striped bar) was used as the standard substrate for the efflux transporters (indicated as a positive control). Bars represent the mean ± S.D. from triplicate runs. Key: *, $p<0.05$; **, $p<0.01$ by one-way ANOVA, followed by Dunnett's *post hoc* test.

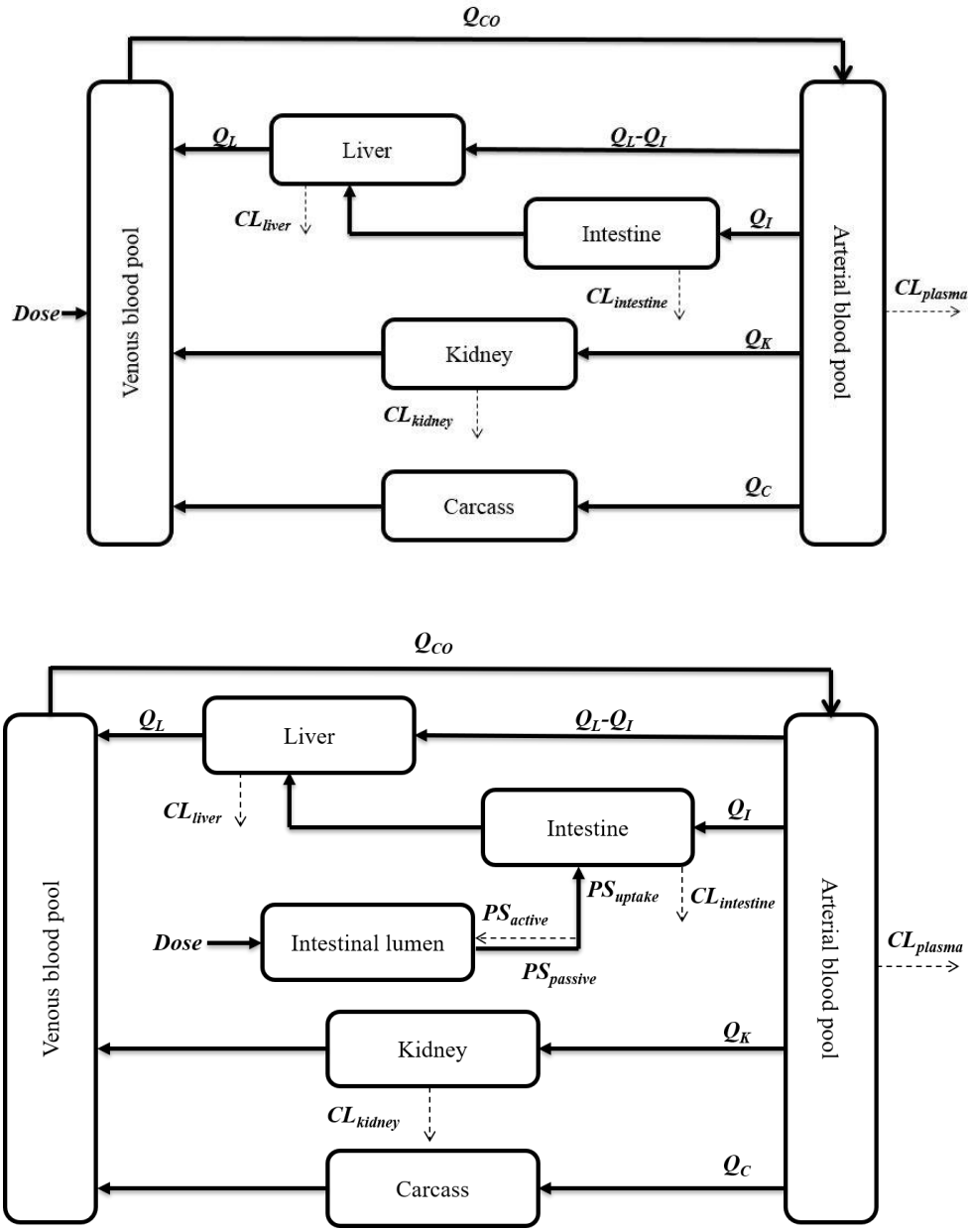

Figure 8. Schematic representation of the PBPK model used in this study for iv or po administration group.

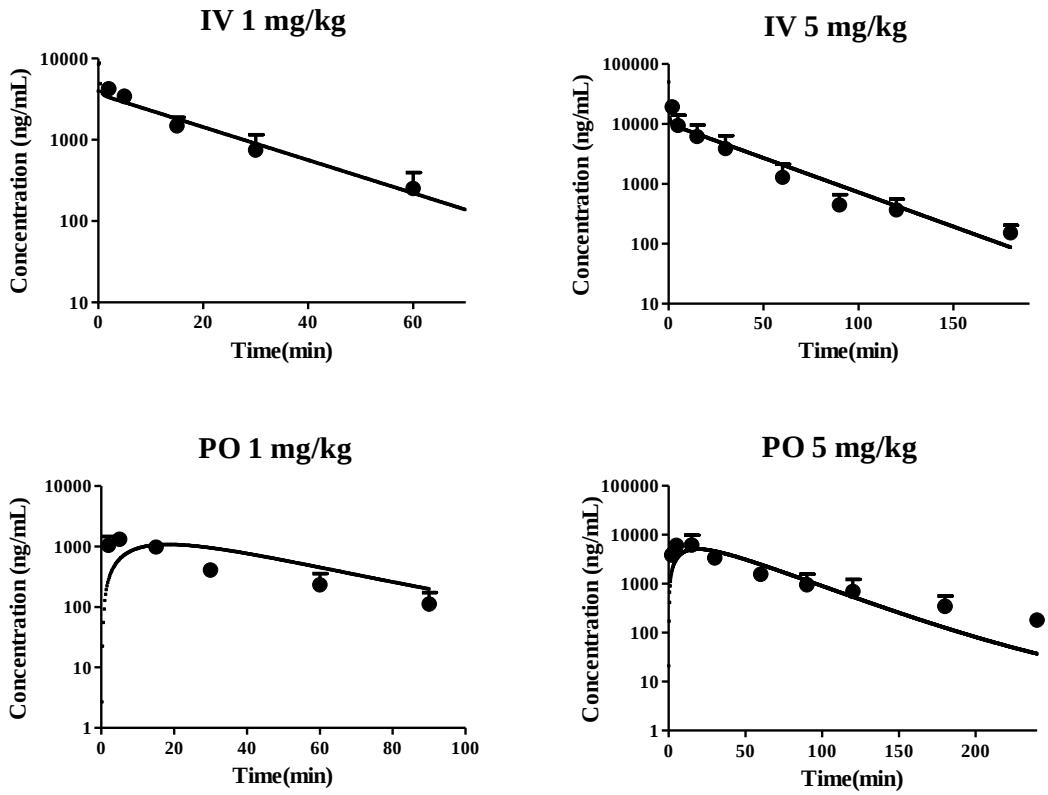

Figure 9. Observed and simulated plasma concentration-time profiles for edaravone after iv or po administration.

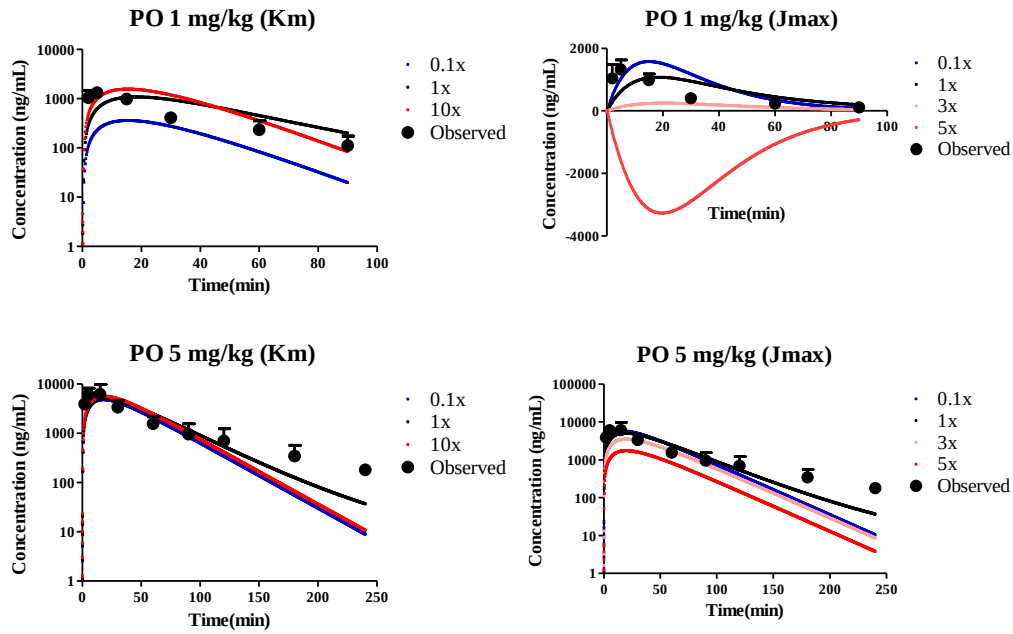

Figure 10. Sensitivity analysis for simulated plasma concentration-time profiles of edaravone.

Blue lines mean the scale less than 1, and red lines mean the scale greater than 1.

APPENDIX

The Conditional Stimulation of Rat Organic Cation Transporter 2, but not its Human Ortholog, by Mesoridazine: The Possibility of the Involvement of the High-Affinity Binding Site of the Transporter in the Stimulation

ABSTRACT

This study was performed to study the conditional stimulation and the species-difference of the organic cation transporter 2 (OCT2) in the presence of phenothiazines, as model organic cations. Madin-Darby canine kidney (MDCKII) cells expressing human or rat OCT2 were established and the kinetics of the transport of N-methyl-4-phenylpyridinium (MPP+), a standard substrate for the transporter, was determined by cellular uptake assays. The concentration dependency was studied for the stimulatory / inhibitory effects of various phenothiazines on the transport of MPP+. Among the 11 commercially available phenothiazine derivatives, the majority (8 of 11) was found to have comparable effects on transporter function between the orthologous forms (i.e., hOCT2 and rOCT2), while three of the phenothiazines, particularly mesoridazine, had complex impacts on transporter function. For the case of rOCT2, mesoridazine stimulated transport at MPP+ concentrations of 0.1 and 1 μM (the substrate concentration lower than K_m value of the substrate) with the mesoridazine concentration-uptake curve becoming bell-shaped (biphasic curve). This conditional effect by mesoridazine became less pronounced at 30 μM MPP+ (the substrate concentration comparable to K_m value of the substrate), resulting in an inhibition curve with a typical profile (i.e., monophasic and sigmoidal shaped profile) for mesoridazine. For the case of hOCT2,

mesoridazine behaved as a typical inhibitor of transporter function at all MPP+ concentrations studied, although the kinetics of inhibition was still affected by the substrate concentration. The conditional stimulation by mesoridazine in the rat form of OCT2, a transporter with multiple binding sites, and the lack thereof in hOCT2, may be a manifestation of the interaction of phenothiazine with substrate binding at the high-affinity site of the OCT2 forms. Since OCT2 was previously indicated in some transporter-mediated drug-drug interactions, the conditional stimulation of the transporter by certain organic cations and its potential species differences may be of practical relevance.

Keywords : Organic cation transporter 2, Drug Transport, Transporter stimulation, Bell-shaped transporter inhibition, Phenothiazines, Species-difference

1. Introduction

The organic cation transporter 2 (OCT2) is found in various organs in the body, including the kidney (Gorboulev et al., 1997), and is believed to be pharmacokinetically relevant in the renal elimination of many cationic drugs (Motohashi et al., 2002). Given the fact that approximately 40% of registered drugs contain amine groups (thus, functioning as cations in the physiological pH range) (Kim and Shim, 2006; Neuhoff et al., 2003), it appears reasonable to expect that a significant frequency of drug-drug interactions may occur between / among cationic drugs if this transporter is involved. As one example, dolutegravir, an antiretroviral drug that blocks the activity of the human immunodeficiency virus, is known to enhance the plasma exposure of metformin, probably by OCT2-mediated interactions that occur during the process of renal elimination (Reese et al., 2013; Song et al., 2016). The United States Food and Drug Administration and other regulatory agencies (e.g., European Medicines Agency and International Transporter Consortium) now recommend that the possibility of drug-drug interactions caused by drug transporters, including OCT2 (Agency, 2012; Huang et al., 2007; International Transporter et al., 2010), should be carefully examined during new drug discovery and development.

In studies directed at identifying a transport pathway and for determining transporter inhibition, the function of the transporter is typically examined using a fixed concentration of its reference substrate in the presence of several concentrations of a test substance as a potential inhibitor. However, this

experimental design may be valid only when the kinetics of inhibition is stationary with reference to the substrate used. It is well known that the cation transporter contains multiple binding sites for some substrates (Gorbunov et al., 2008; Minuesa et al., 2009) [e.g., N-methyl-4-phenylpyridinium (MPP+)]: Theoretically, the transport kinetics can become variable when multiple binding sites are involved, as evidenced by the case of some SLC (e.g., Organic Anion-Transporting Polypeptide (OATP) 1B1 and OATP1B3) (Kindla et al., 2011; Noe et al., 2007; Tamai et al., 2001) and ABC transporters [e.g., Multidrug Resistance-associated Protein (MRP) 2] (Pedersen et al., 2017; Zelcer et al., 2003). For the case of OCT2, the stimulatory effect of some organic cations on OCT2 function varied, depending on the substrate used (Hacker et al., 2015), although the underlying mechanism responsible for this was not fully delineated. Currently, it is not known whether stationary kinetics is adequate for validating the inhibition of OCT2 for certain organic cations.

Species-difference is an important issue in pharmacokinetics studies. In addition to anatomical / physiological differences amongst species (e.g., organ volume, plasma protein binding, and metabolic activity) (Lin, 1995; Mahmood et al., 2003), it is now widely accepted that the kinetics of one type of transporter (e.g., hOCT2) can be different from its orthologous form (e.g., rOCT2) (Chu et al., 2013). The origin of such differences in function may be from differences in the affinity between the substrate and the transporter (related to K_m) and/or from the fact that the transport process between the orthologous forms involve different biophysical mechanisms (related to

V_{max}). These kinetic differences may ultimately lead to distinction(s) in the in vivo kinetics of absorption, distribution and/or excretion between the species (Sabolić et al., 2011; Urakami et al., 1998). For example, it was found that the brain-plasma concentration ratio of [^{11}C]GR205171, an MDR1 substrate, was approximately 9-fold higher in humans than that in rats, probably as the result of functional difference(s) in the transporter between the species (Syvanen et al., 2009).

Following the same line of reasoning, the species-difference could also be related to a dissociation in drug-drug interactions caused by the involvement of orthologous transporters (Tahara et al., 2005; Umehara et al., 2007; Umehara et al., 2008). Furthermore, because of the presence of multiple binding sites for OCT2, species-differences in the function/inhibition of the cation transporter would further complicate the situation. This aspect of OCT2 function has not been systemically studied in the literature.

In our preliminary study with phenothiazine derivatives, organic cations, as potential inhibitors of OCT2, we found certain phenothiazines had complex inhibition profiles for different forms of OCT2. The purpose of this study, therefore, was to examine the inhibitory / stimulatory effects of phenothiazine derivatives on OCT2 functions. We were particularly interested comparing the effect of phenothiazines on the characteristics of orthologous OCT2s from the human and rat, since the pharmacokinetics studies frequently are conducted using those two species. We report herein, for the first time, that three out of 11 phenothiazines derivatives showed complex inhibitory profiles, and that mesoridazine in particular showed a stimulatory profile that

was substrate concentration-dependent. We also report that the inhibitory / stimulatory effects were distinct depending on the species.

2. Materials and Methods

2.1. Materials

N-Methyl-4-phenylpyridinium (MPP+) iodide, diphenhydramine HCl, promethazine HCl, trifluoperazine 2HCl, perphenazine, fluphenazine 2HCl, prochlorperazine dimaleate, mesoridazine benzenesulfonate, promazine HCl, and triflupromazine HCl were purchased from Sigma-Aldrich (St Louis, USA). Chlorpromazine HCl was obtained from Cayman Chemical (Ann Arbor, USA). Thioridazine HCl and mequitazine were also used in this study [both from Tokyo Chemical Industry Co., Ltd. (Tokyo, Japan)]. Radiolabeled [3H] MPP+ (specific activity: 79.8 ~ 80.0 Ci/mmol) was purchased from Perkin Elmer Life or Analytical Sciences (MA, USA). All other chemicals were of the highest grade available and were used without further purification.

2.2. Uptake of MPP+ in OCT2 Expressing MDCKII Cells

In this study, MDCKII-hOCT2, MDCKII-rOCT2, and their corresponding MDCKII-mock cells (i.e., transfection with an empty-vector) were stably generated and the function determined as shown in Supporting Information. When necessary, the accumulation of MPP+ in MDCKII cells (i.e., uptake) was determined using a previously described method, with minor modifications (Jeong et al., 2017; Lee et al., 2015; Yim et al., 2017). Briefly,

MDCKII-hOCT2, MDCKII-rOCT2, and MDCKII-mock cells were grown in Dulbecco's modified Eagle's medium with 10% (v/v) fetal bovine serum, a 1% (v/v) non-essential amino acid solution, 100 units/mL penicillin/streptomycin, and 10 mM HEPES. All cells were kept at 37°C with 5% CO2 and 95% relative humidity. Cells were seeded at the density of 5×10^5 cells/well in poly-L-ornithine (Sigma-Aldrich)-coated 24-well plates [Corning Life Sciences (NY, USA)]. After 3 days, the cells were washed twice with pre-warmed phosphate-buffered saline (PBS) and pre-incubated for 10 min with transport medium (9.7 g/L Hanks' balanced salts, 2.38 g/L HEPES, and 0.35 g/L sodium bicarbonate, pH adjusted to 7.4) at 37°C. Initially, the uptake of MPP+ was measured in 5 min with various concentrations ranging from 0.1 to 500 μM (i.e., 0.1, 1, 10, 30, 50, 100, 500 μM) in hOCT2, rOCT2 and mock cells for the determination of the kinetic constants for MPP+ in the cell system. When it was necessary to study the inhibition profile of phenothiazine derivatives for the OCT2 forms, the compounds were prepared in dimethyl sulfoxide (DMSO) and diluted with transport medium (final DMSO concentrations of 0 ~ 2% depending on the compound). In our previous study, it was found that concentrations of DMSO of up to 2% in the transport medium had no appreciable effect on the function of the MDCKII cells that expressed drug transporter (Yim et al., 2017), consistent with other literature findings (Taub et al., 2002). When DMSO was used as the solvent for the test compounds, an identical amount of the solvent was also included in the control incubation. The cells were pre-warmed at 37°C, and then

incubated for 5 min at 37°C with medium containing various concentrations of phenothiazines (i.e., 0, 1, 3, 10, 30, 100, 300 μM, or 0.3, 1, 3, 10, 30, 100 μM, depending on the solubility, Fig. 1) and radiolabeled [^{3}H]-MPP+, along with unlabeled MPP+ (i.e., to minimize non-specific binding; the total final concentration of MPP to be 1 μM). In some uptake studies, the cells were pre-incubated for 30 min with 30 μM mesoridazine, and MPP+, the substrate, was then added to the mixture for 5 min (Fig. 2) for the uptake assay. After incubation at 37˚C for 5 min, uptake was terminated by aspiration of the transport medium, after which, the cells were immediately washed 3 times with 400 μL of ice-cold PBS. After the last aspiration, an aliquot (500 μL) of 0.2 N NaOH was added to the plate and treated for at least 1 h by vortexing for cell lysis. An aliquot (400 μL) of the lysate was mixed with Ultima Gold (Perkin-Elmer Life Science) 1 mL, and the amount of radiolabeled-substrate accumulated in the cells determined by liquid scintillation counting (Tri-Carb 3110 TR, Perkin-Elmer Life Science). In this study, the uptake of MPP+ was normalized by the total protein concentration, as determined by a BCA assay (Smith et al., 1985), and incubation time (5 min). If necessary, diphenhydramine, a known inhibitor of OCT2, was added to confirm the function of the transporter in cells that were expressing the transporters.

2.3. MTS Assay

To determine whether the presence of phenothiazine derivatives had toxic

effect towards MDCKII cells, an MTS assay was carried out according to the instructions from the manufacturer (Cory et al., 1991). Briefly, MDCKII cells were plated at a density of 13,000 cells per well in a 96-well plate, incubated for at least 24 h to attach/achieve 80~90% confluency. In this study, the confluent cells were treated with the highest concentration of phenothiazine derivative that was used in the uptake studies [i.e., promethazine, trifluoperazine, perphenazine, mesoridazine, promazine, triflupromazine, chlorpromazine, thioridazine, and mequitazine, 300 μM; fluphenazine and prochlorperazine, 100 μM] for 1 h or 2 h, a significantly longer incubation time than that used in the uptake studies (i.e., 5 min). The percentage of viable cells was determined by a CellTiter 96 AQueous Non-Radioactive Cell Proliferation Assay (Promega, Madison, WI, USA) following the manufacturer's protocol. In this study, data were corrected by control cells [i.e., MDCKII cells treated with vehicle (DMSO, final concentration of 0~2%) only].

2.4. hOCT2 and rOCT2 cloning

The open reading frame (ORF) of hOCT2 and rOCT2 were cloned and functionally expressed in MDCKII cells containing Flp-In system, as described in our previous studies (Kim et al., 2010; Lee et al., 2015; Yim et al., 2017). Briefly, hOCT2 and rOCT2 cDNA including coding sequence region (CDS) were amplified by using reverse-transcription PCR method

(Takara, Shiga, Japan) with total RNA from human and rat kidney (Takara, Shiga, Japan). The sets of primer sequence were 5'-TCAGCTGGACCAAGGAAAGGCCC-3' (sense strand), 5'-TTTGCCTAGCCCACAGTTCC-3' (antisense strand) for hOCT2, 5'-ATGTCGACCGTGGATGATAT-3' (sense strand), 5'-CAGGGGTAAGTGAGGTTGG-3' (antisense strand) for rOCT2, and PCR conditions consisted of denaturation in 94°C for 30 sec, annealing in 59°C for 30 sec, and elongation in 72°C for 2 min. The PCR products were assembled into pcDNA5/FRT (Invitrogen, USA). If necessary, the mutations were corrected by using mutagenesis kit (Stratagene, USA), assuming the NCBI registered sequence NM_003058 and NM_031584.2 as the reference sequences for rOCT2 and hOCT2, respectively. In this study, the expressing vectors were analyzed using sequencing (Cosmogenetech, Korea). The OCT2-expressing vectors were transfected using Fugene HD transfection reagent (Promega, Madison, USA) into MDCKII cells modified by Flip-In system (Invitrogen, CA, USA). The transfected cells were incubated in the culture medium containing 0.1 mg/mL hygromycin B (Invitrogen) for two weeks for selection. RT-PCR analyses were carried out to identify the expression of transport systems in MDCKII cells, as described previously (Lee et al., 2015). Briefly, total mRNA was extracted from MDCKII cells using an RNeasy Mini Kit (Qiagen, Valencia, CA, USA) according to the instruction from the manufacturer. After isolation, the concentration and purity of the extracted RNA were confirmed by UV spectrophotometry at

260/280 nm. Reverse transcription and PCR amplification were carried out as mentioned above with same primer sets. The PCR products were separated by gel electrophoresis on 1% (w/v) agarose, inspected under UV light after ethidium bromide staining and photographed with a digital camera (Fig. 5a). The functional activities for MDCKII-hOCT2 and MDCKII-rOCT2 were confirmed by cellular accumulation of substrates, [^{3}H] MPP+ (Wright, 2005), compared with the MDCKII-mock cells (i.e., MDCKII cells transfected with empty vector, control cells), and also by examining the significant depression of the functional activity by the addition of diphenhydramine, reference inhibitor of OCT2 (Muller et al., 2005; Zolk et al., 2009). In this study, at least a 5-fold higher uptake of MPP+ was found for cells expressing hOCT2 and rOCT2 in comparison to that for mock transfected cells (Fig. 5b), indicative of the functional expression in hOCT2 and rOCT2 cells.

2.5. Western Blot

Cells were lysed by incubation in ice-cold lysis buffer (50 mM Tris-HCl, 150 mM NaCl, 1% sodium deoxycholate, 0.1% SDS, 1% Triton X-100, pH=7.5) for 30 min, as followed by being sonicated at 1 sec, five times in ice-cold temperature. The lysate was centrifuged (10,000g, 2 min, 4˚C) and the supernatant collected for the determination of the protein concentration in the lysate as determined by bicinchoninic acid (BCA) assay. The supernatant was added to 2X Laemmli buffer (Bio-Rad, USA) and the mixture boiled for 5

min for protein denaturation. Identical amounts of proteins (6 μg) were loaded on a discontinuous denaturing SDS-PAGE containing 7.5% acrylamide and were separated by electrophoresis (Bio-Rad, USA). Proteins were transferred onto nitrocellulose membrane (Bio-Rad, USA). Nonspecific-binding of the antibody was inhibited by incubating the membranes with blocking buffer containing skim-milk (Biosesang, Korea) for 1 h. The membranes were, then, incubated with a rabbit polyclonal antibody [Anti-SLC22A2, Sigma-Aldrich, diluted 1:1000 with Tris-buffered saline containing 0.05% tween and 5% skim-milk] raised against a peptide mapping OCT2, for overnight at 4˚C. After washing the membranes three times with the Tris-buffer, the peroxidase-coupled second antibody (Cell Signaling Technology, diluted 1:2000 with Tris-buffered saline containing 0.05% tween) was added onto membranes. Similar method was used to show anti-glyceraldehyde 3-phosphate dehydrogenase (GADPH) bands with Anti-GAPDH (Cell Signaling Technology, USA) as positive controls. Chemiluminescent signals were visualized by using an enhanced chemiluminescence solution (Bio-Rad, USA) and LAS4000 digital imagining system (GE Healthcare Life Sciences, Pittsburgh, PA, USA) (Fig. 5c).

2.6. Data Analysis

For the determination of kinetic parameters for MPP+ transport in MDCKII

cells, parallel passive and carrier-mediated transport processes (equation 1) were assumed to be applicable;

$$V = \frac{V_{max} \times [S]}{K_m + [S]} + P_{diff} \times [S] \ldots\ldots\ldots equation\ (1)$$

where [S] is the substrate concentrations, V_{max} is the maximal rate of MPP+ uptake, K_m is the substrate concentration at half-maximal transport velocity, and P_{diff} is the rate constant for passive diffusion. To obtain the kinetic parameters, V_{max}, K_m, and P_{diff}, the data were fitted to equation 1 by nonlinear regression analysis (see below).

When it was necessary to determine the IC_{50} for phenothiazine derivatives, the transport was assumed to be explained by the following equation,

$$V = V_{max} - (V_{max} - V_0) \times \left[\frac{[I]^n}{[I]^n + (IC_{50})^n}\right] \ldots\ldots\ldots equation\ (2)$$

where V is the rate of MPP+ uptake (5 min) in the presence of the inhibitor, V_0 is the basal rate of MPP+ uptake, [I] is the concentration of the potential inhibitor, IC_{50} is the concentration of the inhibitor at half-maximal transport velocity, and n is the Hill coefficient. The data were fitted to equation 2 to obtain kinetic parameters (V_{max}, V_0, IC_{50} and n) by nonlinear regression analysis (see below).

When it was necessary to convert IC_{50} to K_i, the Cheng-Prusoff equation

(equation 3) was used (Yung-Chi and Prusoff, 1973) under the assumption that competitive inhibition existed between MPP+ and phenothiazine derivatives;

$$K_i = \frac{IC_{50}}{(\frac{[S]}{K_m} + 1)} \ldots\ldots\ldots equation\ (3)$$

To compare the means between treatments, two-tailed, unpaired Student's t test or one-way ANOVA was used. When it was necessary to compare the means amongst groups after the ANOVA test, Dunnett's post hoc test was used. When necessary, nonlinear regression analysis and other statistical analyses were carried out using GraphPad Prism version 5.01 (GraphPad Software Inc., San Diego, CA). In this study, data are expressed as the mean ± S.D. and a $p<0.05$ was accepted as denoting statistical significance.

3. Results

3.1. Confirmation of the Functional Expression of OCT2 Transporters in MDCKII Cells and Estimation of Optimal Conditions for an Uptake Assay

From our preliminary studies, both forms of OCT2 were found to be stably expressed in MDCKII cells (Fig. 5) after the transfection. MPP+ uptake, as determined by cellular accumulation, was enhanced in MDCKII cells expressing hOCT2 or rOCT2 in comparison to their mock cells in 5 min of the transport reaction (Fig. 5b). A temporal profile of transport indicates that cellular accumulation (i.e., uptake) increased proportionally with time up to 5 min and then reached a plateau at approximately 10 min after initiation (Fig. 6a): In subsequent studies, a 5 min incubation time was used. The concentration dependency for uptake indicates that the transport of MPP+ in these MDCKII cells may be explained by parallel passive and saturable processes (Fig. 6b), consistent with the Eadie-Hofstee transformation of the data (data not shown). A nonlinear regression analysis with equation 1 indicated that K_m values for MPP+ in MDCKII-hOCT2 and MDCKII-rOCT2 cells were 39.8 ± 12.1 μM, and 50.5 ± 10.4 μM, respectively. These values were not statistically different from each other, indicating that the affinities for MPP+ transport were comparable between the two forms of OCT2 in MDCKII cells. In this study, the maximal velocities, V_{max}, for MPP+ transport

in hOCT2 and rOCT2 cells [in pmol/(mg protein*min)] were determined to be 2500 ± 525 and 3360 ± 1020, respectively. The K_i values for inhibiting MPP+ uptake by diphenhydramine in hOCT2 and rOCT2 cells were 11.2 ± 6.69 μM and 15.4 ± 8.70 μM, respectively (Fig. 6c). Again, no statistical difference in K_i was found for the inhibition of MPP+ transport by the inhibitor between OCT2 transporters from the two species. Furthermore, these kinetic estimates were consistent with values reported in the literature (Muller et al., 2005; Zolk et al., 2009), indicating that the functional expression of h/rOCT2 transporters in the experimental system and the transport assay are adequate.

3.2. Screening for Stimulatory Effects of Phenothiazine Derivatives in MDCKII Cells Expressing OCT2 Transporters

To determine whether the complex inhibitory response(s) of phenothiazine derivatives exist, 11 commercially available phenothiazine derivatives were obtained and their effects screened (Fig. 1). We were particularly interested in determining whether species-differences in the inhibition/stimulation of the cation transporter existed for these derivatives. Amongst the phenothiazine derivatives, trifluoperazine, fluphenazine, perphenazine, prochloroperazine, and thioridazine had no effect on the function of the h/rOCT2 transporters. In the case of phenothiazines such as promazine and chlorpromazine, these compounds inhibited both MDCKII-hOCT2 and MDCKII-rOCT2 to a

comparable extent without any apparent abnormality (Table 1). Promethazine showed a species-difference in the inhibitory kinetic constants toward the uptake of MPP+, although the phenothiazine did not stimulate the transport in the concentration range studied. Mequitazine and trifluprom azine were weakly stimulatory for the functions of hOCT2 and rOCT2, respectively. Amongst the phenothiazines tested, the stimulatory effect was most pronounced for mesoridazine in rOCT2 (Fig. 1). Therefore, in subsequent studies, we focused on the kinetics of rOCT2 stimulation by mesoridazine and on comparing these with the function of hOCT2.

3.3. Kinetic Comparison of Function of h/rOCT2 Transporters in the Presence of Mesoridazine

When MDCKII-rOCT2 cells were treated with mesoridazine at 30 μM for 5 min, the uptake of MPP+ was significantly enhanced (i.e., Fig. 2, 180 ± 35.2 % of the function for control group, $p<0.01$). The observation was similar to that obtained for pre-incubation with mesoridazine for 30 min (i.e., Fig. 2, 186 ± 7.19 % of the function for the control group, $p<0.01$). Interestingly, stimulation was not apparent at higher concentrations of mesoridazine in MDCKII-rOCT2, suggesting that the stimulatory effect may be masked at that level of concentration (Fig. 1a). As a result, the profile for MPP+ uptake-mesoridazine concentration appeared to be biphasic (i.e., bell-shaped), probably because of the fact that mesoridazine conditionally

stimulates the function of rOCT2 depending on the concentration of the phenothiazine (i.e., stimulation at lower concentrations, inhibition at higher concentration).

Because of the potential involvement of conditional stimulation, a kinetic characterization of the inhibition (i.e., estimation of IC_{50} and K_i) was not possible for mesoridazine for rOCT2, in most cases. In the case of hOCT2, the uptake of MPP+ was inhibited in the entire concentration range of mesoridazine with no apparent stimulation (Fig. 1a). Accordingly, the IC_{50} and K_i values of hOCT2 for inhibiting MPP+ transport (substrate concentration of 1 μM) by mesoridazine were estimated to be 100 ± 9.56 μM, with a K_i value of 97.7 ± 9.33 μM, respectively.

To study the conditional stimulation of OCT2 by mesoridazine, MPP+ transport was compared at the varying substrate concentrations in the presence and absence of a fixed concentration of mesoridazine at 30 μM (i.e., the mesoridazine concentration showing the most pronounced stimulation, Fig. 1a) in MDCKII cells expressing rOCT2 (Fig. 3). In this comparative study, the experiment was repeated on three different days for statistical analysis. MPP+ uptake was apparently enhanced (Fig. 3a, $p<0.01$ at an MPP+ concentration of 0.1 μM) in the presence of mesoridazine when the uptake was compared with that in its absence at lower concentrations of MPP+. In contrast, transport with the treatment was reduced ($p<0.05$ at all MPP+ concentrations greater than 50 μM, Fig. 3a) in comparison to that without the treatment (Fig. 3a) at a higher MPP+ concentration. As a result, when the ratio

of uptake in the presence of mesoridazine to that in the absence was calculated and plotted against the concentration of MPP+, the correlation had a negative slope (i.e., -0.389, $p<0.0001$) and the ratio at an MPP+ concentration at 1 μM was 1.461, which was greater than 1 (one sample t test, $p<0.0001$) (Fig. 3b). In addition, one-way ANOVA indicated that the averaged ratio was statistically different ($p<0.05$) with respect to MPP+ concentration: In particular, the averaged ratio at 0.1 μM MPP+ was significantly different ($p<0.05$, Dunnett's post hoc test) to that at 500 μM. Taken together, these statistical analyses indicate that the effect of mesoridazine is conditional with respect to the MPP+ (i.e., the substrate) concentration (i.e., stimulatory for MPP+ transport at lower concentrations of the substrate and becoming inhibitory at higher concentrations) and that the inhibitory kinetics is not stationary for the substrate concentration used.

To further examine the relationships between MPP+ and mesoridazine in influencing the function of h/rOCT2, the uptake of MPP+ at three different substrate concentrations was studied with varying concentrations of mesoridazine (Fig. 4). Again, the phenothiazine appeared to act as an inhibitor of the uptake of MPP+ in cells expressing hOCT2 at all three substrate concentrations (Fig. 4a), although the IC_{50} and K_i for the uptake of mesoridazine at 30 μM MPP+ tended to be reduced (no statistical difference for IC_{50}, $p<0.05$ for K_i by Dunnett's post hoc test) when the kinetic parameters were compared with those at lower MPP+ concentrations (Table 2). For the case of rOCT2 cells, mesoridazine enhanced uptake at the concentrations

below 30 μM of mesoridazine in MDCKII-rOCT2 (Fig. 4b) at MPP+ concentrations equal to or lower than 1 μM, consistent with previous observations (Fig. 3a). However, the transport study with 30 μM MPP+ (i.e., concentration close to the MPP+ K_m), the stimulatory effect of mesoridazine was absent and the compound appeared to behave as a typical inhibitor of MPP+ transport (Fig. 3a). Assuming that the profile can be explained by simple competitive inhibition kinetics at the highest concentration of MPP+, equations 2 and 3 were used to analyze the kinetics using nonlinear regression. The IC_{50} and K_i for mesoridazine (inhibitor) at 30 μM MPP+ (substrate) were estimated, respectively (Table 2).

In this study, the possibility of cellular damage occurring in MDCKII cells was examined, particularly for any cellular damage that could lead to a non-specific effect of stimulation/inhibition in MPP+ transport (Table 3). An MTS assay indicated that the exposure of 11 phenothiazines at the highest concentration for 2 h used in the transport studies, generally had no appreciable effect on cellular viability (data not shown). However, for the case of promazine and trifluprom azine, cellular toxicity was noted at 2 h, although this toxic effect disappeared when the exposure time was reduced to 1 h. In comparison, the exposure of MDCKII cells to phenothiazines was limited to 5 min in our transport studies. Therefore, this observation indicates that the interaction of the cation transporter with the above phenothiazines is not related to non-specific/toxic effects.

4. Discussion

One of the objectives of the current study was to examine the functional outcome of rat and human forms of OCT2 in the presence of phenothiazine derivatives, particularly mesoridazine. We found that a stimulatory response was consistently observed with mesoridazine for rOCT2 at concentrations of 30 μM or less. In the literature, conditional stimulation of transporter function was noted in transporters other than OCT2. For example, in a study using pravastatin as the substrate, diclofenac was reported to enhance the OATP1B3-mediated uptake of pravastatin at lower concentrations, while substrate uptake was reduced at higher concentrations of diclofenac (Kindla et al., 2011). Unfortunately, however, the study mainly focused on differences in the affinity of diclofenac, rather than characterizing the allosteric nature of the stimulation. In addition to the example with OATP1B3, indomethacin was reported to enhance MRP2-mediated methotrexate transport with a similar conditional stimulation profile (Zelcer et al., 2003). Furthermore, it was reported in the literature that some phenothiazines stimulated the efflux of 2',7'-Bis-(3-carboxypropyl)-5-(and-6)-carboxyfluorescein acetoxymethyl ester (BCPCF), a substrate of MRP1, from human hepatocytes, while they could also inhibit the function of P-gp (Wesolowska et al., 2009). Furthermore, phenothiazine maleate was also reported to increase the function of MRP1 (Wesolowska et al., 2005). From these literatures (Wesolowska et al., 2009; Wesolowska et al., 2005; Zelcer et al., 2003), it was

proposed that the stimulator(s) may interact with MRP1 at a site different from the substrate binding site and modulate the function of the transporter. It was also proposed that the same compound (i.e., the stimulator), at a different concentration range, may directly interact with the substrate binding site thereby functioning as an inhibitor, consistent with the bell-shaped curve for this function. It therefore appears that the biphasic (i.e., stimulatory at low concentrations while inhibitory at high concentrations) behavior of activity modulators may not be uncommon in some SLC and ABC transporters.

In the literature, organic cation transporters (Gorbunov et al., 2008), including OCT2, were reported to have multiple binding sites available for substrates (Koepsell, 2015; Minuesa et al., 2009). The concerted action between two different binding sites of MPP+ (i.e., substrate transport at the low-affinity site while a modulatory role at the high-affinity site) was previously proposed in the literature (Gorbunov et al., 2008; Minuesa et al., 2009), consistent with our observation that a mesoridazine treatment enhanced the transport of OCT2 at lower concentrations of MPP+. Therefore, it is possible that the conditional response may be a manifestation of interactions of phenothiazine with multiple binding sites (e.g., the binding of mesoridazine at the high-affinity site leading to enhanced MPP+ transport; the binding of the phenothiazine at the low-affinity transported site leading to reduced MPP+ transport). In support of this hypothesis, we were able to obtain a K_i value only when the MPP+ concentration was increased to 30 μM, close to the K_m value (i.e., apparently a typical inhibition profile with mesoridazine; Fig. 4b).

This observation also suggests that the high-affinity site in rOCT2 is sufficiently saturated by MPP+ at concentrations of 30 μM or more. In contrast, the response of mesoridazine became biphasic (i.e., stimulation of transport at a lower concentration of mesoridazine while inhibition at a higher concentration) when MPP+ transport was examined at MPP+ concentrations of 0.1 or 1 μM (Fig. 4b). To our knowledge, this is the first demonstration of a biphasic response (i.e., stimulatory at a certain concentration range while inhibitory at concentrations outside the range) in OCT2 function with phenothiazines. It was previously reported for some organic cations that the stimulation of OCT2 varied, depending on the substrate (Hacker et al., 2015): In this study, we evaluated the Tanimoto similarity factor (T) (Willett et al., 1998) between mesoridazine and compounds that stimulated hOCT2 (Hacker et al., 2015) by using ChemMine (Girke et al., 2005) to determine the molecular similarity. When the criteria of similarity was limited to T>0.25, only benperidol and mirtazapine showed relatively high molecular similarities with mesoridazine. Although molecular similarity may not guarantee a similar biological activity (Martin et al., 2002), additional studies directed at evaluating OCT2 with those molecularly similar compounds may be necessary. This variability (i.e., substrate dependency) may be explained by the current hypothesis that the high-affinity site is modulatory for the transport function. The biophysical mechanism for the interaction between substrate/inhibitor and the transporter is not currently completely clear for OCT transporters. However, the mechanism(s) responsible for the transport

appears to be similar to that of the rOCT1 model derived from lactose permease of Escherichia coli (Egenberger et al., 2012; Popp et al., 2005), suggesting the existence of a common translocation mechanism for the various forms of OCT2 with respect to substrate translocation. It was proposed in the literature that the mechanism for the transport of OCTs might be explained by one cation /monomer transport mode or two cation/monomer transport mode (Koepsell, 2015). According to this proposal, the inhibitory effect of OCTs would be dependent on the substrate concentration: At low substrate concentrations, an inhibitor may interact, not only with the site occupied by the substrate, but also with the unoccupied substrate binding site located in the vicinity. This scenario explains the dissociation in the inhibitory effect (i.e., IC_{50}) of an inhibitor in OCT2-mediated transport with different substrates (Belzer et al., 2013; Thevenod et al., 2013). At a concentration above its K_m value, both of substrate binding sites would be expected to be occupied so that the inhibitory effects of the compound would not be affected by substrates. For the modulatory domain of OCT transporters, however, the role of the high-affinity binding site of OCT2 has not been systemically studied in the literature. To understand the role of the high-affinity binding sites of the substrate, and the species-differences of OCT2, biophysical aspects of the mechanism responsible for transport need to be understood for OCTs (Gorbunov et al., 2008; Koepsell, 2015; Volk et al., 2009).

Another crucial finding of the current study is that the response to the function was species-dependent. The stimulatory response was detected only in a

certain concentration range for mesoridazine in rOCT2. In contrast, no stimulation was apparently detected in any of the concentrations studied for the case of hOCT2. However, a closer examination of the data for hOCT2 indicate that the K_i value at 30 μM MPP+ is reduced ($p<0.05$, one-way ANOVA followed by Dunnett's post hoc test) compared to those at lower concentrations. Although the underlying mechanism was not directly investigated in this study, we speculate that mesoridazine participates in a weak interaction at the high-affinity binding site in hOCT2, leading to a relatively obscure stimulatory effect that only affected the estimation of K_i. At higher concentrations of MPP+, i.e. at 30 μM, the high-affinity site may be fully saturated by MPP+, thus lowering the estimated value for the K_i. Obviously, other non-specific mechanisms for the non-stationary kinetics cannot be excluded, based on the findings reported herein (e.g., a change in the binding of mesoridazine by a high concentration of MPP+ at the surface of the cell, thereby leading to a lower K_i or the existence of one or two cation/monomer transport modes) (Koepsell, 2015). Additional studies are clearly warranted for developing a complete understanding of the factors responsible for the change in the kinetics of inhibition for OCT2-mediated transport of MPP+ by mesoridazine. Regardless of the underlying mechanism(s), however, our data indicate that the assumption of stationary kinetics is invalidated for the inhibition of OCT2 transporters, both the rat and human forms, by mesoridazine.

From our data and other literature reports, it became apparent that studies of

transporter-mediated drug-drug interactions should be considerably more elaborate in their design: At least three transport systems appear to be associated with biphasic responses for certain substrates/inhibitors. In particular, it is noteworthy that transporter interaction could be rendered ambiguous due to the kinetic complexity (i.e., stimulation in transport at certain inhibitor concentrations but inhibition at different concentrations). Therefore, kinetic analyses with multiple concentration levels of substrates as well as potential inhibitors are likely warranted for an accurate assessment of inhibitor kinetics.

To determine whether the stimulatory response in the function of OCT2 was prevalent for phenothiazines in general, 11 commercially available phenothiazines were studied in connection with transport via rOCT2 and hOCT2. In particular, these phenothiazines could be used as model compounds in studies, given the fact that they are all organic cations and are structurally similar. Indeed, it was previously reported in the literature that several phenothiazines had inhibitory effects on the functions of the OCT2 transporter (Hacker et al., 2015; Haenisch et al., 2012; Zolk et al., 2009). To the best of our knowledge, however, the current study represents the first attempt to define and comprehensively study the interaction between phenothiazines and OCT2 using an identical experimental system. We found that, among 11 phenothiazines, 5 (trifluoperazine, fluphenazine, perphenazine, prochloroperazine and thioridazine) had no effect on the function of both OCT2 forms, while 4 (triflupromzine, chlorpromazine,

promazine and mequitazine) showed comparable levels of inhibition for both transporters at high concentrations. Among these compounds, mequitazine and trifluprom azine showed slight biphasic stimulation at low concentrations, although the complex response was not as obvious as that for mesoridazine. In addition to mesoridazine, species-differences in inhibitory effects for OCT2 were also noted for promethazine. Interestingly, when the substrate concentration was increased to 30 μM, a species-difference for promethazine was still observed: In addition, this phenothiazine derivative did not stimulate OCT2 functions in our experiments. Collectively, the molecular site responsible for the species-differences for promethazine is probably unrelated to the modulatory site(s) of MPP+ in OCT2. Because of the limited number of phenothiazine derivatives that show a species-difference, it is not possible to propose a crucial chemical feature of the molecule for the difference. Interestingly, however, phenothiazines that contain amine groups linked to the -N side of the phenothiazine ring appeared to interact with OCT2, as indicated in Fig. 7. In addition, those phenothiazines having a piperazine group (i.e., trifluoperazine, fluphenazine, perphenazine, and prochloroperazine) did not interact with OCT2 functions. Trifluprom azine, chlorpromazine, and promazine, i.e., derivatives with a 3-(N,N-dimethylamino)propan structure, inhibited both forms of OCT2. It is possible that functional groups linked to the 2-carbon of the phenothiazine backbone also affect OCT2 interactions. Additional characterizations will be necessary for a further understanding of the species-difference to be developed in terms

of chemical structure.

5. Conclusion

A biphasic stimulation response was found for rOCT2 function in the presence of mesoridazine, probably because of the interaction of the phenothiazine with multiple binding sites of the transporter. Although a clear biphasic response by mesoridazine was not observed for hOCT2 function, the inhibition kinetics were dependent on the concentration of the substrate, suggesting that the stationary kinetics cannot be assumed for the inhibition of OCT2 when MPP+ is used as the substrate. The biphasic response of the function of OCT2, along with a species-difference, found in the study may be practically important, particularly in the characterization of the potential drug-drug interactions that involve OCT2 transporters.

6. References

EMA., 2012. Guideline on the investigation of drug interactions. Committee for Human Medicinal Products (CHMP).

Belzer, M., et al., 2013. Substrate-dependent ligand inhibition of the human organic cation transporter OCT2. Journal of Pharmacology and Experimental Therapeutics 346, 300-310.

Bussow, K., 2015. Stable mammalian producer cell lines for structural biology. Current Opinion in Structural Biology 32, 81-90.

Chu, X., et al., 2013. Species differences in drug transporters and implications for translating preclinical findings to humans. Expert Opinion on Drug Metabolism and Toxicology 9, 237-252.

Cory, A.H., et al., 1991. Use of an aqueous soluble tetrazolium formazan assay for cell-growth assays in culture. Cancer Communications 3, 207-212.

Egenberger, B., et al., 2012. A substrate binding hinge domain is critical for transport-related structural changes of organic cation transporter 1. Journal of Biological Chemistry 287, 31561-31573.

Girke, T., et al., 2005. ChemMine. A compound mining database for chemical genomics. Plant Physiology 138, 573-577.

Gorboulev, V., et al., 1997. Cloning and characterization of two human polyspecific organic cation transporters. DNA and Cell Biology 16, 871-881.

Gorbunov, D., et al., 2008. High-affinity cation binding to organic cation transporter 1 induces movement of helix 11 and blocks transport after

mutations in a modeled interaction domain between two helices. Molecular Pharmacology 73, 50-61.

Hacker, K., et al., 2015. Substrate-dependent inhibition of the human organic cation transporter OCT2: a Comparison of metformin with experimental substrates. PLoS One 10, e0136451.

Haenisch, B., et al., 2012. Interaction of antidepressant and antipsychotic drugs with the human organic cation transporters hOCT1, hOCT2 and hOCT3. Naunyn-Schmiedeberg's Archives of Pharmacology 385, 1017-1023.

Huang, S.M., et al., 2007. Drug interaction studies: study design, data analysis, and implications for dosing and labeling. Clinical Pharmacology & Therapeutics 81, 298-304.

International Transporter, C., et al., 2010. Membrane transporters in drug development. Nature Reviews. Drug Discovery 9, 215-236.

Jeong, Y.S., et al., 2017. Estimation of the minimum permeability coefficient in rats for perfusion-limited tissue distribution in whole-body physiologically-based pharmacokinetics. European Journal of Pharmaceutics and Biopharmaceutics 115, 1-17.

Kim, M.H., et al., 2010. Evidence of carrier-mediated transport in the penetration of donepezil into the rat brain. Journal of Pharmaceutical Sciences 99, 1548-1566.

Kim, M.K., Shim, C.K., 2006. The transport of organic cations in the small intestine: current knowledge and emerging concepts. Archives of Pharmacal Research 29, 605-616.

Kindla, J., et al., 2011. Influence of non-steroidal anti-inflammatory drugs on organic anion transporting polypeptide (OATP) 1B1- and OATP1B3-mediated drug transport. Drug Metabolism and Disposition 39, 1047-1053.

Koepsell, H., 2015. Role of organic cation transporters in drug-drug interaction. Expert Opinion on Drug Metabolism and Toxicology 11, 1619-1633.

Lee, J.H., et al., 2015. Kinetics of the absorption, distribution, metabolism, and excretion of lobeglitazone, a novel activator of peroxisome proliferator-activated receptor gamma in rats. Journal of Pharmaceutical Sciences 104, 3049-3059.

Lin, J.H., 1995. Species similarities and differences in pharmacokinetics. Drug Metabolism and Disposition 23, 1008-1021.

Mahmood, I., et al., 2003. Selection of the first-time dose in humans: comparison of different approaches based on interspecies scaling of clearance. Journal of Clinical Pharmacology 43, 692-697.

Martin, Y.C., et al., 2002. Do structurally similar molecules have similar biological activity? Journal of Medicinal Chemistry 45, 4350-4358.

McLeod, M., et al., 1986. Identification of the crossover site during FLP-mediated recombination in the Saccharomyces cerevisiae plasmid 2 microns circle. Molecular and Cellular Biology 6, 3357-3367.

Minuesa, G., et al., 2009. Transport of lamivudine [(-)-beta-L-2',3'-dideoxy-3'-thiacytidine] and high-affinity interaction of nucleoside reverse transcriptase inhibitors with human organic cation transporters 1, 2, and 3.

Journal of Pharmacology and Experimental Therapeutics 329, 252-261.

Motohashi, H., et al., 2002. Gene expression levels and immunolocalization of organic ion transporters in the human kidney. Journal of the American Society of Nephrology 13, 866-874.

Muller, J., et al., 2005. Drug specificity and intestinal membrane localization of human organic cation transporters (OCT). Biochemical Pharmacology 70, 1851-1860.

Neuhoff, S., et al., 2003. pH-dependent bidirectional transport of weakly basic drugs across Caco-2 monolayers: implications for drug-drug interactions. Pharmaceutical Research 20, 1141-1148.

Noe, J., et al., 2007. Substrate-dependent drug-drug interactions between gemfibrozil, fluvastatin and other organic anion-transporting peptide (OATP) substrates on OATP1B1, OATP2B1, and OATP1B3. Drug Metabolism and Disposition 35, 1308-1314.

Pedersen, J.M., et al., 2017. Substrate and method dependent inhibition of three ABC-transporters (MDR1, BCRP, and MRP2). European Journal of Pharmaceutical Sciences 103, 70-76.

Popp, C., et al., 2005. Amino acids critical for substrate affinity of rat organic cation transporter 1 line the substrate binding region in a model derived from the tertiary structure of lactose permease. Molecular Pharmacology 67, 1600-1611.

Reese, M.J., et al., 2013. In vitro investigations into the roles of drug transporters and metabolizing enzymes in the disposition and drug

interactions of dolutegravir, a HIV integrase inhibitor. Drug Metabolism and Disposition 41, 353-361.

Sabolić, I., et al., 2011. Are mice, rats, and rabbits good models for physiological, pharmacological and toxicological studies in humans? Periodicum Biologorum 113, 7-16.

Smith, P.K., et al., 1985. Measurement of protein using bicinchoninic acid. Analytical Biochemistry 150, 76-85.

Song, I.H., et al., 2016. The effect of dolutegravir on the pharmacokinetics of metformin in healthy subjects. Journal of Acquired Immune Deficiency Syndromes 72, 400-407.

Syvanen, S., et al., 2009. Species differences in blood-brain barrier transport of three positron emission tomography radioligands with emphasis on P-glycoprotein transport. Drug Metabolism and Disposition 37, 635-643.

Tahara, H., et al., 2005. A species difference in the transport activities of H2 receptor antagonists by rat and human renal organic anion and cation transporters. Journal of Pharmacology and Experimental Therapeutics 315, 337-345.

Tamai, I., et al., 2001. Functional characterization of human organic anion transporting polypeptide B (OATP-B) in comparison with liver-specific OATP-C. Pharmaceutical Research 18, 1262-1269.

Taub, M.E., et al., 2002. Optimized conditions for MDCK permeability and turbidimetric solubility studies using compounds representative of BCS classes I–IV. European Journal of Pharmaceutical Sciences 15, 331-340.

Thevenod, F., et al., 2013. Substrate- and cell contact-dependent inhibitor affinity of human organic cation transporter 2: studies with two classical organic cation substrates and the novel substrate cd2+. Molecular Pharmaceutics 10, 3045-3056.

Umehara, K.I., et al., 2007. Comparison of the kinetic characteristics of inhibitory effects exerted by biguanides and H2-blockers on human and rat organic cation transporter-mediated transport: Insight into the development of drug candidates. Xenobiotica 37, 618-634.

Umehara, K.I., et al., 2008. Effect of cationic drugs on the transporting activity of human and rat OCT/Oct 1-3 in vitro and implications for drug-drug interactions. Xenobiotica 38, 1203-1218.

Urakami, Y., et al., 1998. Functional characteristics and membrane localization of rat multispecific organic cation transporters, OCT1 and OCT2, mediating tubular secretion of cationic drugs. Journal of Pharmacology and Experimental Therapeutics 287, 800-805.

Volk, C., et al., 2009. Five amino acids in the innermost cavity of the substrate binding cleft of organic cation transporter 1 interact with extracellular and intracellular corticosterone. Molecular Pharmacology 76, 275-289.

Wesolowska, O., et al., 2009. Differential effect of phenothiazines on MRP1 and P-glycoprotein activity. In Vivo 23, 943-947.

Wesolowska, O., et al., 2005. Phenothiazine maleates stimulate MRP1 transport activity in human erythrocytes. Biochimica et Biophysica Acta 1720, 52-58.

Willett, P., et al., 1998. Chemical similarity searching. Journal of Chemical Information and Computer Sciences 38, 983-996.

Wright, S.H., 2005. Role of organic cation transporters in the renal handling of therapeutic agents and xenobiotics. Toxicology and Applied Pharmacology 204, 309-319.

Yim, C.S., et al., 2017. Specific inhibition of the distribution of lobeglitazone to the liver by atorvastatin in rats: evidence for a rat organic anion transporting polypeptide 1B2-mediated interaction in hepatic transport. Drug Metabolism and Disposition 45, 246-259.

Yung-Chi, C., Prusoff, W.H., 1973. Relationship between the inhibition constant (Ki) and the concentration of inhibitor which causes 50 per cent inhibition (I50) of an enzymatic reaction. Biochemical Pharmacology 22, 3099-3108.

Zelcer, N., et al., 2003. Evidence for two interacting ligand binding sites in human multidrug resistance protein 2 (ATP binding cassette C2). Journal of Biological Chemistry 278, 23538-23544.

Zolk, O., et al., 2009. Structural determinants of inhibitor interaction with the human organic cation transporter OCT2 (SLC22A2). Naunyn-Schmiedeberg's Archives of Pharmacology 379, 337-348.

Table 1. IC_{50} and K_i values for phenothiazines in MDCKII-hOCT2 or MDCKII-rOCT2 cells at a substrate (MPP+) concentration of 1 μM (5 min uptake).

Inhibitors	IC_{50} (μM)		K_i (μM)		P value*
	hOCT2	rOCT2	hOCT2	rOCT2	
Promethazine	27.1 ± 22.4	130 ± 56.8	26.4 ± 21.8	128 ± 55.7	< 0.05
Chlorpromazine	79.3 ± 15.9	89.6 ± 29.2	77.4 ± 15.6	87.8 ± 28.6	N.S
Mequitazine	43.9 ± 3.31	34.4 ± 14.2	42.8 ± 3.23	33.7 ± 13.9	N.S
Promazine	15.1 ± 8.27	9.09 ± 2.72	14.8 ± 8.07	8.91 ± 2.67	N.S
Triflupromazine	69.7 ± 22.6	85.6 ± 35.7	68.0 ± 22.0	84.0 ± 35.0	N.S

Data are expressed as the mean ± S.D. from triplicate runs in triplicate determinations.

* P values were obtained by two-tailed, unpaired Student's t test.

Table 2. IC_{50} and K_i values for mesoridazine on the uptake of MPP+ at 0.1, 1, and 30 μM in the MDCKII-hOCT2 or MDCKII-rOCT2 cells (5 min uptake).

	IC_{50}			K_i		
	0.1 μM	1 μM	30 μM	0.1 μM	1 μM	30 μM
hOCT2	92.6 ± 44.3	100 ± 9.56	45.5 ± 2.74	92.4 ± 44.2	97.7 ± 9.33	25.9 ± 1.56*,#
rOCT2	-	-	57.7 ± 13.2	-	-	36.2 ± 8.24

Data are expressed as the mean ± S.D. from triplicate runs in triplicate determinations.

*, $p<0.05$ with 1 μM; #, $p<0.05$ with 0.1 μM by one-way ANOVA, followed by Dunnett's post hoc test.

Table 3. Viability of MDCKII cells in the presence of stimulatory phenothiazines as measured by an MTS assay.

Time	Viability (% of control)			
	Control	Mesoridazine	Promazine	Trifluprom azine
1 h	100 ± 6.67	113 ± 6.04	99.9 ± 10.4	89.6 ± 4.22
2 h	100 ± 3.02	109 ± 11.7	77.5 ± 7.46*	67.8 ± 4.55**

Data are expressed as the mean ± S.D. from triplicate runs.

*, $p<0.05$; **, $p<0.01$ with control by one-way ANOVA, followed by Dunnett's post hoc test.

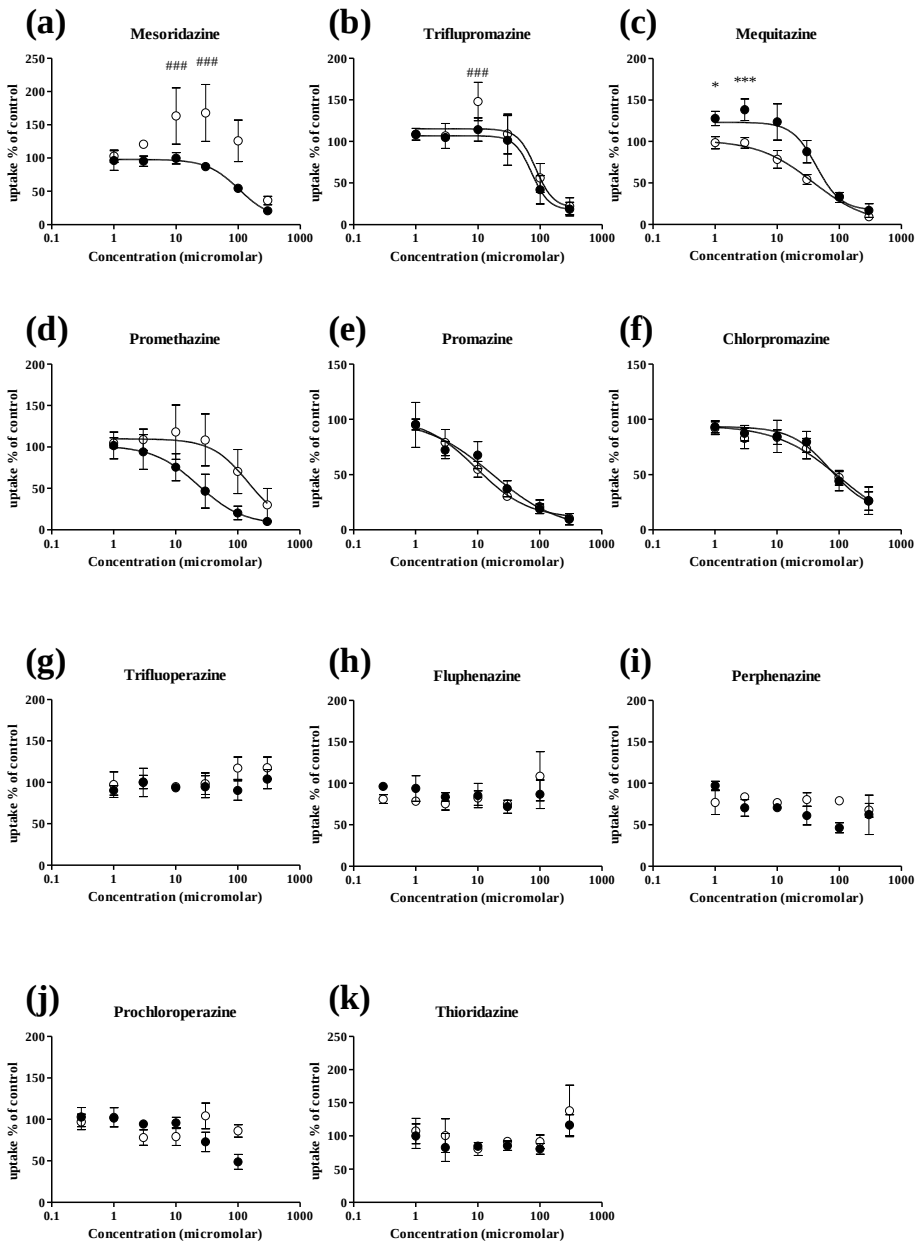

Figure 1. Concentration-dependent uptake of MPP+ in the presence of phenothiazine derivatives.

(a) mesoridazine, (b) trifluprom azine, (c) mequitazine, (d) promethazine, (e) promazine, (f) chlorpromazine, (g) trifluoperazine, (h) fluphenazine, (i)

perphenazine, (j) prochloroperazine, and (k) thioridazine in MDCKII-hOCT2(●) or MDCKII-rOCT2(○) cells. Cells were incubated at 37˚C for 5 min with 1 μM MPP+ in the presence of phenothiazines (1, 3, 10, 30, 100, 300 μM, except for fluphenazine and prochloroperazine; for these two phenothiazines, 0.3, 1, 3, 10, 30, 100 μM) (pH=7.4). The uptake rate was normalized by the value obtained in the absence of phenothiazines in each assay. Data points represent the mean ± S.D. from triplicate runs in triplicate determinations (i.e., experiments run on three different days; each day, three different determinations for the concentration levels). Key: *, $p<0.05$; ***, $p<0.001$ for hOCT2, #, $p<0.05$; ###, $p<0.001$ for rOCT2 by one-way ANOVA, followed by Dunnett's post hoc test. Asterisks (*, for hOCT2) and number signs (#, for rOCT2) represent apparent difference for the comparative function of >100%.

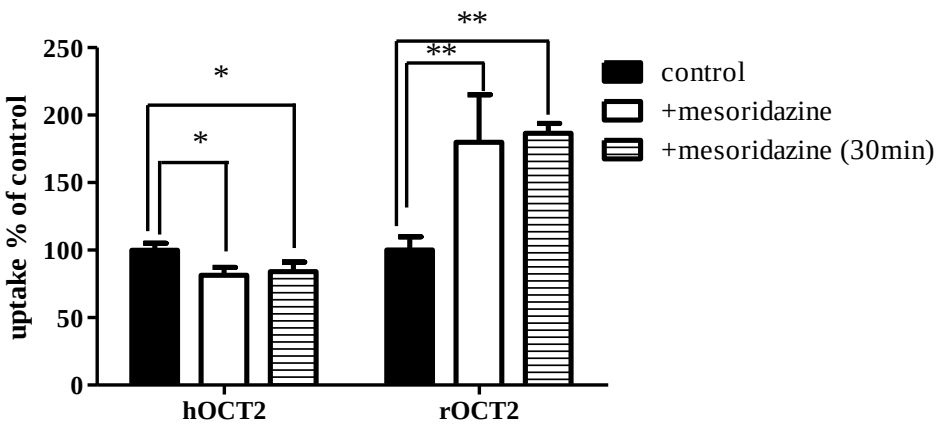

Figure 2. Uptake of MPP+ by MDCKII-hOCT2 and MDCKII-rOCT2 cells with mesoridazine.

The rate of MPP+ uptake was determined in MDCKII-hOCT2 or MDCKII-rOCT2 cells with 30 μM mesoridazine via co-treatment (i.e., blank bars) or a 30 min pre-incubation (i.e., striped bars). In this figure, the results from control experiment (i.e., without mesoridazine treatment/pre-incubation) are also presented (i.e., filled bars) Bars represent the mean ± S.D. of triplicate runs. Key: *, $p<0.05$; **, $p<0.01$ by one-way ANOVA, followed by Dunnett's post hoc test.

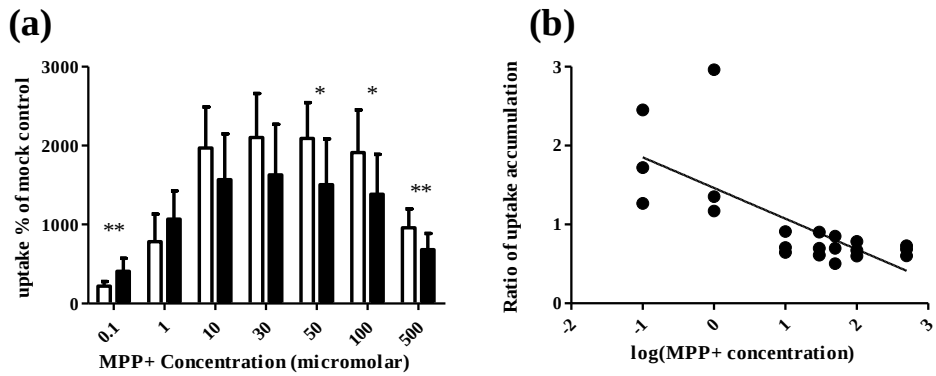

Figure 3. Substrate concentration-dependent bi-phasic stimulation of OCT2 by mesoridazine.

(a) Concentration-dependent uptake of MPP+ in MDCKII-rOCT2 with mesoridazine treatment. MPP+ uptake (37˚C, 5 min) was determined at various concentrations (0.1, 1, 10, 30, 50, 100, 500 μM) with (i.e., filled bars) or without (i.e., blank bars) 30 μM mesoridazine (pH=7.4). Data are expressed as the mean ± S.D. from triplicate runs in triplicate determinations (i.e., experiments run on three different days; each day, three different determinations for the concentration levels). Key: *, $p<0.05$; **, $p<0.01$ by two-tailed, unpaired Student's t test. (b) Concentration-dependency of the ratio of the MPP+ uptake rate between control and mesoridazine 30 μM treatment with respect to MPP+ concentration. Data points represent the ratio calculated for each day at given concentration level.

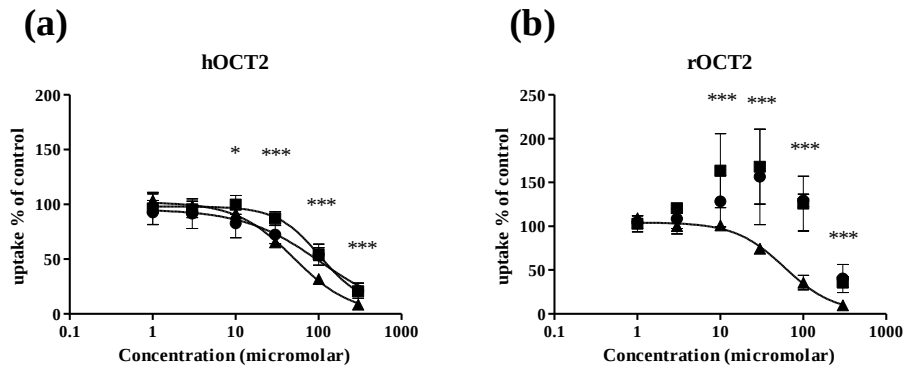

Figure 4. Uptake of MPP+ at three different substrate concentrations in the presence of mesoridazine in MDCKII cells expressing OCT2 transporters. Cells were incubated at 37˚C for 5 min with 0.1(●), 1(■), or 30(▲) μM MPP+ in the presence of mesoridazine (1, 3, 10, 30, 100, 300 μM) (pH=7.4). The uptake rate was normalized by the value obtained in the absence of mesoridazine in each assay. Data are expressed as the mean ± S.D. from triplicate runs in triplicate determinations (i.e., experiments run on three different days; each day, three different determinations for the concentration levels). Key: *, $p<0.05$; ***, $p<0.001$ by one-way ANOVA, followed by Dunnett's post hoc test.

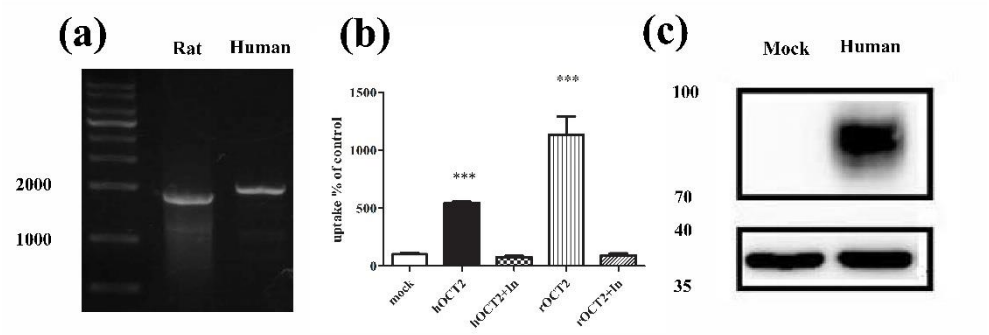

Figure 5. Establishment of MDCKII-hOCT2 and MDCKII-rOCT2 cell line and its determinations.

(a) Agarose gel electrophoresis of RT-PCR product using the primers with the total RNA extract from MDCKII cell line expressing the corresponding transporter. The numbers in the most left lane represent the expected molecular size of the band (bp). (b) The functional expression of hOCT2 or rOCT2 in MDCKII cells. MPP+ (1 μM) was treated at 5 min at 37˚C (pH=7.4). Diphenhydramine was used as representative inhibitor. Bars represent the mean ± S.D. (n=3). ***, $p<0.001$ by one-way ANOVA, followed by Dunnett's post hoc test. (c) Characterization of the expression of hOCT2 in MDCKII-hOCT2 cells by Western blot. MDCKII-mock (empty vector) cells were used as negative control. GAPDH expression data were shown as positive control. The numbers in the most left lane represent the expected molecular size of the band (kDa).

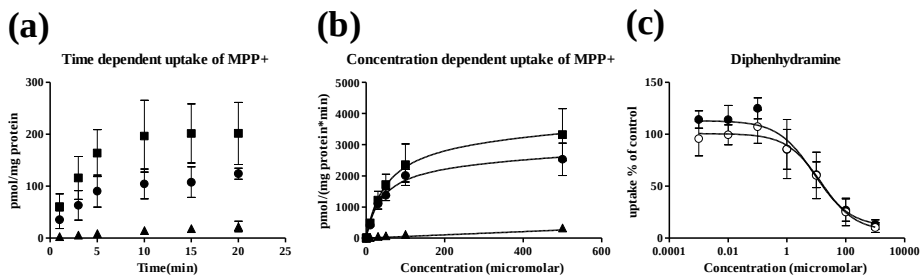

Figure 6. Optimization of experimental design for MDCKII-hOCT2 and MDCKII-rOCT2 cell line.

(a) Time-dependent uptake profile of MPP+ by MDCKII-hOCT2(●), MDCKII-rOCT2(■) and MDCKII-mock (▲). MPP+ (1 μM) was treated at various incubation times (1, 3, 5, 10, 15, 20 min) at 37˚C (pH=7.4). Data points represent the mean ± S.D. from triplicate runs in triplicate determinations (i.e., experiments run on three different days; each day, three different determinations). (b) Concentration-dependent uptake profile of MPP+ by MDCKII-hOCT2(●), MDCKII-rOCT2(■) and MDCKII-mock(▲). MPP+ uptake was determined at 37 ˚C for 5min at various concentrations (0.1, 1, 10, 30, 50, 100, 500 μM) (pH=7.4). Data points represent the mean ± S.D. from triplicate runs in triplicate determinations. (c) Inhibitory effects of diphenhydramine, used as reference inhibitor, for uptake of MPP+ in MDCKII-hOCT2(●) or MDCKII-rOCT2(○), at the various concentrations (0.001, 0.01, 0.1, 1, 10, 100, 1000 μM). Data points represent the mean ± S.D. from triplicate runs in triplicate determinations.

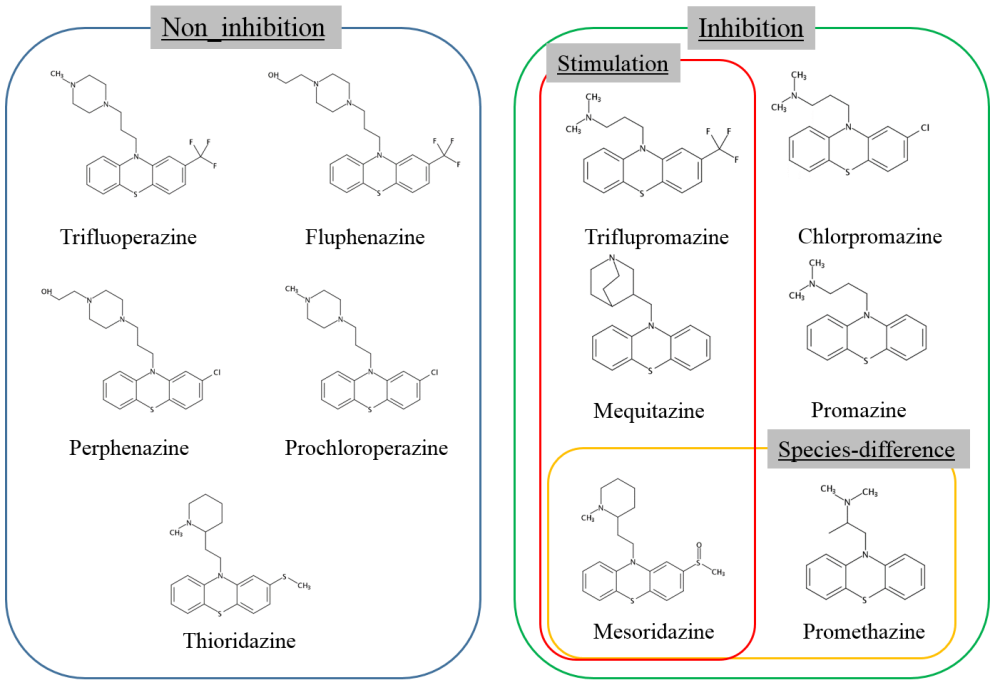

Figure 7. Chemical structures of phenothiazine derivatives used in OCT2 interaction studies.

The compounds were categorized by the observation of OCT2 inhibition at high concentrations (300 μM). Groups that showed stimulation or species-difference were also categorized.